www.nature.com/cdd

CDDpress

ARTICLE

Check for updates

FAAH served a key membrane-anchoring and stabilizing role for NLRP3 protein independently of the endocannabinoid system

Yangyang Zhu[1,2,8], Hao Zhang[1,2,8], Huawei Mao[3,8], Suqin Zhong[1,2], Yubing Huang[2], Sirong Chen[2], Kai Yan[4], Zhibin Zhao[4], Xiaohan Hao[2], Yue Zhang[3], Han Yao[5], Xiaowan Huang[2], Meimei Wang[1,2], Wenbin Zhang[2], Juan Li[6], Guangxun Meng[6], Xiaohua Qin[1,2], Zhiming Ye[4], Jiani Shen[4], Yang Song[1,2], Youcui Xu[4], Zhenyu Yang[7], Liansheng Wang[1,4✉], Yunjiao Zhang[2✉] and Longping Wen[1,4✉]

NLRP3, the sensor protein of the NLRP3 inflammasome, plays central roles in innate immunity. Over-activation of NLRP3 inflammasome contributes to the pathogenesis of a variety of inflammatory diseases, while gain-of-function mutations of NLRP3 cause cryopyrin-associated periodic syndromes (CAPS). NLRP3 inhibitors, particularly those that inhibit inflammasome assembly and activation, are being intensively pursued, but alternative approaches for targeting NLRP3 would be highly desirable. During priming NLRP3 protein is synthesized on demand and becomes attached to the membranes of ER and mitochondria. Here, we show that fatty acid amide hydrolase (FAAH), the key integral membrane enzyme in the endocannabinoid system, unexpectedly served the critical membrane-anchoring and stabilizing role for NLRP3. The specific interaction between NLRP3 and FAAH, mediated by the NACHT and LRR domains of NLRP3 and the amidase signature sequence of FAAH, was essential for preventing CHIP- and NBR1-mediated selective autophagy of NLRP3. Heterozygous knockout of FAAH, resulting in ~50% reduction in both FAAH and NLRP3 expression, was sufficient to substantially inhibit the auto-inflammatory phenotypes of the NLRP3-R258W knock-in mice, while homozygous FAAH loss almost completely abrogates these phenotypes. Interestingly, select FAAH inhibitors, in particular URB597 and PF-04457845, disrupted NLRP3–FAAH interaction and induced autophagic NLRP3 degradation, leading to diminished inflammasome activation in mouse macrophage cells as well as in peripheral blood mononuclear cells isolated from CAPS patients. Our results unraveled a novel NLRP3-stabilizing mechanism and pinpointed NLRP3–FAAH interaction as a potential drug target for CAPS and other NLRP3-driven diseases.

Cell Death & Differentiation (2023) 30:168–183; https://doi.org/10.1038/s41418-022-01054-4

INTRODUCTION

Inflammasomes are multiprotein signaling platforms that operate to drive inflammation in response to exogenous or endogenous danger signals [1–3]. Among the multiple distinct inflammasomes identified, the NLRP3 inflammasome has gained the most attention, as aberrant NLRP3 inflammasome activity contributes to the pathogenesis of a vast number of human diseases [4–6]. In addition to NLRP3 as a sensor, the NLRP3 inflammasome also contains an adaptor (ASC) and an effector (caspase-1). Upon the assembly of the NLRP3 inflammasome, caspase-1 is cleaved, leading to the activation and release of the pro-inflammatory cytokines IL-1β and IL-18, as well as to gasdermin D-mediated pyroptosis [7–9]. A tripartite protein, NLRP3 consists of a pyrin domain (PYD) in the amino terminus, a NACHT domain in the middle and a leucine-rich repeat domain (LRR domain) in the carboxy terminus. Mutations in and around the NACHT domain of NLRP3, rendering NLRP3 constitutively active, cause cryopyrin-associated periodic syndromes (CAPS), a spectrum of diseases including familial cold auto-inflammatory syndrome (FCAS), Muckle Wells syndrome (MWS) and neonatal onset multisystem inflammatory disorder (NOMID) [10–13]. CAPS-associated NLRP3 mutations have been proposed to manifest conformational changes for the protein, resulting in an inflammasome capable of responding to reduced amounts of activating factors [14].

As dysregulated NLRP3 inflammasome activity drives the progression of many diseases, it is critical for NLRP3 inflammasome

[1]Guangdong Provincial People's Hospital & Guangdong Academy of Medical Sciences, School of Medicine, South China University of Technology, Guangzhou, China. [2]School of Medicine & Institute for Life Sciences, South China University of Technology, Guangzhou, China. [3]Department of Immunology, National Center for Children's Health, Beijing Children's Hospital of Capital Medical University, Beijing, China. [4]Department of Nephrology, Medical Research Center, Guangdong Cardiovascular Institute, Guangdong Provincial People's Hospital & Guangdong Academy of Medical Sciences, Guangzhou, China. [5]Institute of Molecular Medicine, Renji Hospital, Shanghai Jiao Tong University School of Medicine, Shanghai, China. [6]The Center for Microbes, Development and Health, CAS Key Laboratory of Molecular Virology& Immunology, Institut Pasteur of Shanghai, Chinese Academy of Sciences, Shanghai, China. [7]China-Singapore International Joint Research Institute, Guangzhou, China. [8]These authors contributed equally: Yangyang Zhu, Hao Zhang, Huawei Mao. ✉email: wangliansheng@gdph.org.cn; zhangyunjiao@scut.edu.cn; lpwen@ustc.edu.cn

Edited by C. Borner

Received: 11 January 2022 Revised: 11 August 2022 Accepted: 22 August 2022
Published online: 14 September 2022

to be kept in check. In accordance with this principle, the NLRP3 protein in the cells is normally maintained at a very low level that is insufficient for activation. In a process termed "priming", recognition of danger-associated molecular patterns or pathogen-associated molecular patterns by pattern-recognition receptors triggers the synthesis of large quantities of NLRP3, but the inflammasome assembly still does not occur unless the cells receive an additional activating signal [1, 15]. Given this delicate "two signal" controlling mechanism, ensuring that NLRP3-initiated inflammation is turned on only when absolutely necessary, it is reasonable to propose that the NLRP3 protein is inherently unstable. In agreement with this premise, NLRP3 has been shown to undergo ubiquitination-dependent degradation through either the proteasome or autophagy pathway under different circumstances [16–18], with deubiquitinases such as the UAF1/USP1 complex and USP19 serving important roles in stabilizing NLRP3 [19, 20]. Moreover, the NLRP3 molecules before inflammasome assembly are reportedly located on the membranes of ER and mitochondria [21–23], placing NLRP3 in a convenient location to rapidly sense inflammatory signals, but the anchoring molecules remain poorly understood. MAVS, cardiolipin, mitofusin 2 and STING have all been shown to anchor NLRP3 to either mitochondria or ER or both [24–27], but these molecules are likely to serve the proposed anchoring role only upon inflammasome activation or under specific circumstances such as during viral infection.

Fatty acid amide hydrolase (FAAH), a member of a large and diverse class of enzymes referred to as the amidase signature (AS) family and an integral membrane protein, degrades various endogenous signaling lipids including the endocannabinoid anandamide (AEA) and other fatty acid amides (FAAs), thus modulating numerous physiological processes such as pain, feeding, blood pressure, mood, and behavior [28–30]. Ample evidence indicates that FAAH is also closely associated with inflammation, and loss of FAAH, through either pharmacological or genetic inhibition, exerts an anti-inflammatory effect [31–33]. Moreover, URB597, a FAAH inhibitor, was reported to alleviate CCH-induced NLRP3 inflammasome activation by promoting the restoration of lysosomal function [34]. Notably, the anti-inflammatory action conferred by FAAH loss is generally attributed to an increase, as a result of reduced FAAH enzymatic activity, in the level of its substrates such as AEA, which has been shown to inhibit l-homocysteine-induced NLRP3 inflammasome activation in podocytes [35]. However, whether FAAH could affect NLRP3 inflammasome in an endocannabinoid-independent manner has not been reported. Here, we reveal an unexpected role of FAAH in anchoring NLRP3 to both ER and mitochondria membranes and stabilizing NLRP3.

RESULTS

Loss of FAAH specifically inhibited NLRP3 inflammasome activation

To assess the potential role of FAAH in NLRP3 inflammasome activation, we knocked down FAAH in the mouse bone marrow-derived macrophages (BMDMs) using shRNA (Fig. S1a). This led to a significant reduction in the secretion of cleaved caspase-1 and IL-1β triggered by Nigericin following LPS priming (Fig. 1a, b). To systematically study the impact of FAAH loss, we created FAAH knockout mice (Fig. S1b–e). Consistent with the published report [36], $FAAH^{-/-}$ mice had reduced FAAH enzymatic activity and elevated AEA content in the brain (Fig. S2a, b). Upon AEA challenge, $FAAH^{-/-}$ mice displayed enhanced hypothermal response and reduced pain sensitivity (Fig. S2c–e). $FAAH^{-/-}$ mice also exhibited reduced reproduction capacity, as reported [37], while $FAAH^{+/-}$ mice reproduced normally. Compared to $FAAH^{+/+}$ BMDMs, $FAAH^{+/-}$ and $FAAH^{-/-}$ BMDMs exhibited a reduction of 45% and 68%, respectively, in the Nigericin-triggered IL-1β release as determined by ELISA (Fig. 1c). A consistent result was obtained by Western blotting (Fig. 1d). In addition, loss of FAAH reduced Nigericin-induced IL-18 release and pyroptotic cell death (Fig. 1e, f), but had little impact on poly (dA:dT) activation of AIM2 and Salmonella activation of NLRC4 inflammasomes (Fig. 1g), indicating a specific effect of FAAH on NLRP3 inflammasome. Heterozygous and homozygous loss of FAAH also reduced serum IL-1β by ~45% and 70%, respectively, after systemic LPS administration (Fig. 1h) without affecting serum TNF-α (Fig. S2f). Furthermore, in an monosodium urate (MSU)-induced periodontitis model, neutrophil infiltration and IL-1β release were increased in the $FAAH^{+/+}$ mice as expected, but this response was significantly reduced in the $FAAH^{+/-}$ and $FAAH^{-/-}$ mice (Fig. 1I, j). Kupffer cells isolated from the $FAAH^{-/-}$ mice displayed little increase of NLRP3 protein after LPS priming (Fig. 1k) and an 88% reduction in IL-1β release upon Nigericin challenge (Fig. 1l), suggesting a higher impact of FAAH loss on NLRP3 in Kupffer cells than in BMDMs.

Loss of FAAH also inhibited the auto-inflammatory phenotype of NLRP3-R258W mice

To assess the impact of FAAH loss on mutant NLRP3, we generated NLRP3-R258W (referred to as R258W hereafter) $FAAH^{+/-}$ and R258W $FAAH^{-/-}$ mice. In the BMDMs isolated from these mice, heterozygous and homozygous loss of FAAH respectively decreased IL-1β release by 39% and 64% after LPS treatment (Fig. 2a, b), which alone was sufficient to activate CAPS-mutated NLRP3 inflammasome, as compared to R258W $FAAH^{+/+}$ BMDMs. R258W mice gained weight more slowly than the wild-type NLRP3 mice, but loss of FAAH largely abrogated this growth-retarding effect elicited by the R258W mutation (Fig. 2c). Heterozygous loss of FAAH was sufficient to reduce short stature, hair loss and skin inflammation observed with R258W mice, while homozygous FAAH knockout almost completely reverted these phenotypes (Fig. 2d). $FAAH^{+/+}$ R258W mice also showed enlarged axillary lymph node, spleen and liver, while these organs excised from $FAAH^{+/-}$ R258W and $FAAH^{-/-}$ R258W mice were significantly smaller, with only slight difference seen between the wildtype and $FAAH^{-/-}$ R258W mice (Figs. 2e, S3a–c). Histologic study of the affected skin revealed thickening and heavy neutrophil infiltration in both epidermis and dermis of $FAAH^{+/+}$ R258W mice, while these features were largely absent for $FAAH^{+/-}$ R258W and $FAAH^{-/-}$ R258W mice (Fig. 2f). The dermis of $FAAH^{+/+}$ R258W mice was nearly three times as thick as that of the wildtype mice, but remarkably, both heterozygous and homozygous loss of FAAH completely abrogated this phenotype (Fig. 2f, right panel). In addition, the axillary lymph nodes showed germinal center architecture disturbance, follicular dysplasia, and a diffuse neutrophil invasion, whereas the liver exhibited a marked periductal leukocyte infiltration and the spleen contained expanded red pulp areas filled with neutrophils and islands of trilineage hematopoietic cells, but these features were nearly absent in the $FAAH^{+/-}$ R258W and $FAAH^{-/-}$ R258W mice (Fig. S3d to f). Similar results on immune cell infiltration in the axillary lymph nodes and spleen were revealed by immunohistochemistry and T-distributed stochastic neighbor embedding (t-SNE) analysis of multi-parameter flow cytometry (Fig. 2g, h, Fig. S3g). Taken together, the above results demonstrated that the heterozygous loss of FAAH substantially inhibited, while homozygous loss of FAAH almost completely abrogated, the inflammatory phenotype manifested by NLRP3-R258W mutation.

Loss of FAAH induced selective autophagy of NLRP3 protein

To understand how the loss of FAAH led to diminished NLRP3 inflammasome activation, we focused on macrophages, the primary target cells of NLRP3 inflammasome. FAAH deficiency had little effect on either NLRP3 mRNA level or NF-kB pathway activation (Fig. S4a, b), but decreased NLRP3 protein level (Fig. 3a). While LPS priming increased NLRP3 protein in a time-dependent

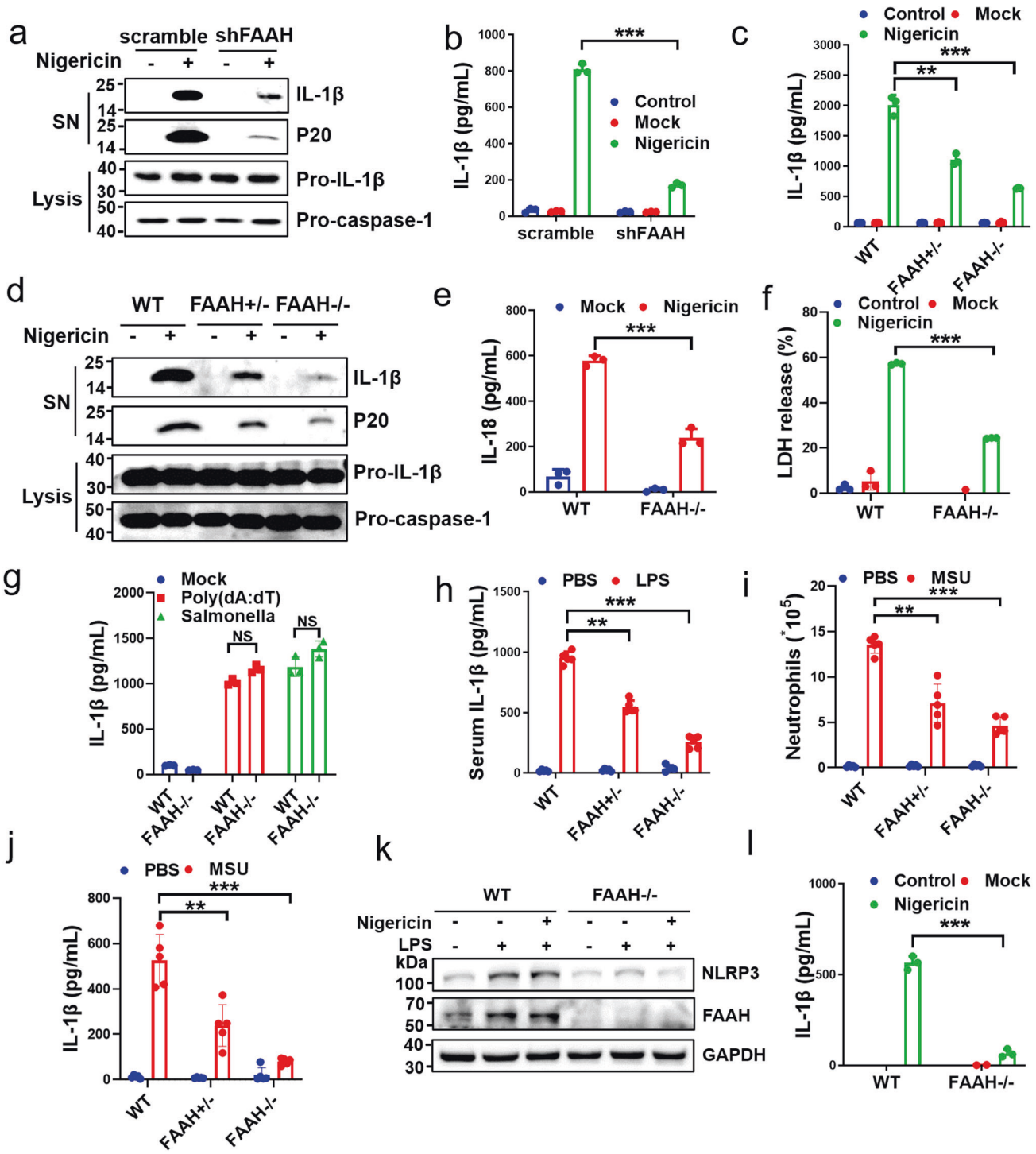

fashion in BMDMs, FAAH knockout resulted in a relatively lower NLRP3 protein level at all of the time points, with the lowest level observed in the *FAAH*$^{-/-}$ cells (Fig. 3b, with a representative Western blot shown in Fig. S4c). Furthermore, loss of FAAH accelerated the reduction of NLRP3 protein in the presence of protein synthesis inhibitor cycloheximide (Fig. 3c, Fig. S4c), pinpointing enhanced protein degradation as the underlying cause for the decreased protein level. Autophagy inhibitors 3-MA, chloroquine (CQ) and wortmannin, as well as knockdown of ATG5, increased NLRP3 protein level in LPS-primed *FAAH*$^{-/-}$ BMDMs (Fig. 3d, e), indicating autophagy-mediated NLRP3 degradation. In contract, proteasomal inhibitors MG132, PS341 and b-AP15 further decreased NLRP3 level in these cells (Fig. S4d), suggesting enhanced autophagic degradation upon proteasomal inhibition. Since NLRP3 degradation in the *FAAH*$^{-/-}$ BMDMs exhibited high specificity, with no decrease in the level of NLRC4, AIM2, NEK7 and ASC (Fig. S5a), we speculated that this degradation proceeded via selective autophagy, a process accomplished through delivery of ubiquitinated cargos to autophagosomes by specific autophagy receptors [38]. In support, the deubiquitylation inhibitor PR619 increased, while the ubiquitination inhibitor PYR41 decreased, NLRP3 degradation in *FAAH*$^{-/-}$ BMDMs (Fig. 3f). Moreover, NLRP3

Fig. 1 Loss of FAAH induced NLRP3 degradation. a Immunoblot of IL-1β and cleaved caspase-1 (p20) in culture supernatants (SN) and pro-caspase 1 and pro-IL-1β in the cell lysate (lysis). Mouse BMDMs were transfected with scrambled or FAAH-specific shRNA, LPS primed for 3 h, followed by Nigericin challenge for 30 min. **b** ELISA of IL-1β in supernatants of mouse BMDMs that have been transfected with scrambled or FAAH-specific shRNA. The cells were unstimulated (Control), LPS-primed (Mock) for 3 h or LPS-primed followed by Nigericin challenge for 30 min (Nigericin). Mean ± SEM, $n = 3$, $^{***}p < 0.001$. **c** ELISA of IL-1β in supernatants of BMDMs from wildtype, $FAAH^{+/-}$ and $FAAH^{-/-}$ mice. The cells were unstimulated (Control), LPS-primed for 3 h (Mock) or LPS-primed followed by Nigericin challenge for 30 min. Mean ± SEM, $n = 3$, $^{**}p < 0.01$; $^{***}p < 0.001$. **d** Immunoblot analysis showing IL-1β and cleaved caspase-1 (p20) in culture supernatants (SN), and pro-caspase 1 and pro-IL-1β in the cell lysate (lysis), of wildtype, $FAAH^{+/-}$ and $FAAH^{-/-}$ BMDMs that were LPS-primed for 3 h followed with or without Nigericin challenge for 30 min. **e** ELISA of IL-18 in supernatants of BMDMs from wildtype and $FAAH^{-/-}$ mice. The cells were LPS-primed for 3 h (Mock) or LPS-primed for 3 h followed by Nigericin challenge for 30 min. Mean ± SEM, $n = 3$, $^{***}p < 0.001$. **f** LDH release in BMDMs from wildtype and $FAAH^{-/-}$ mice. The cells were unstimulated (Cont), LPS-primed for 3 h (Mock) or LPS-primed for 3 h followed by Nigericin challenge for 30 min. Mean ± SEM, $n = 3$, $^{***}p < 0.001$. **g** ELISA of IL-1β in supernatants of wildtype and $FAAH^{-/-}$ BMDMs that were LPS-primed for 3 h (Mock) and LPS-primed followed by Poly(dA:dT) or Salmonella challenge for 4 h. Mean ± SEM, $n = 3$, NS, non-significant. **h** ELISA of IL-1β in the serum of wildtype or $FAAH^{-/-}$ mice 4 h after intraperitoneal injection of PBS or LPS (25 mg/kg). Mean ± SEM, $n = 3$, $^{**}p < 0.01$; $^{***}p < 0.001$. **i** FACS analysis of neutrophil numbers in the peritoneal cavity of wildtype, $FAAH^{+/-}$ and $FAAH^{-/-}$ mice intraperitoneally injected with MSU (50 mg/kg). Mean ± SEM, $n = 3$, $^{**}p < 0.01$; $^{***}p < 0.001$. NS non-significant. **j** ELISA of IL-1β in the peritoneal cavity of wildtype, $FAAH^{+/-}$ and $FAAH^{-/-}$ mice, 6 h after intraperitoneal injection of MSU (50 mg/kg). Mean ± SEM, $n = 3$, $^{**}p < 0.01$; $^{***}p < 0.001$. NS non-significant. **k**, **l** Immunoblot analysis (**k**) and ELISA of IL-1β in supernatants (**l**) of Kupffer cells isolated from wildtype and $FAAH^{-/-}$ mice. The cells were unstimulated (Control), LPS-primed for 3 h (Mock) or LPS-primed followed by Nigericin challenge for 30 min. Mean ± SEM, $n = 3$, $^{***}p < 0.001$.

exhibited enhanced K48, but not K63, ubiquitination upon FAAH loss (Fig. 3g, Fig. S5b). MARCH7 and CHIP are the two E3 ligases implicated in dopamine-induced selective autophagy of NLRP3 in macrophages [18]. Consistent with the reported results, neither CHIP nor MARCH7 interacted with NLRP3 in the wildtype BMDMs. However, upon loss of FAAH, CHIP, but not MARCH7, became bound to NLRP3 (Fig. 3h, Fig. S5c). Furthermore, knockdown of CHIP reduced NLRP3 degradation incurred by FAAH deficiency (Fig. 3i). To identify the autophagy receptor involved, we assessed p62, NBR1 and NDP52. NBR1 and NDP52, but not p62, exhibited increased interaction with NLRP3 in $FAAH^{-/-}$ BMDMs (Fig. S5d). However, only the knockdown of NBR1 reduced NLRP3 degradation (Fig. 3j, Fig. S5e). Thus, loss of FAAH induced degradation of NLRP3 through selective autophagy mediated by CHIP as the E3 ligase and NBR1 as the autophagy receptor.

FAAH interacted with and stabilized NLRP3 independently of FAAH's enzymatic activity

A critical question is whether the NLRP3-destabilizing effect under FAAH loss was mediated by endocannabinoids. Expression of the full-length FAAH in $FAAH^{-/-}$ BMDMs (Fig. S6a), while producing a threefold increase in FAAH enzymatic activity (Fig. 4a), fully "rescued" the capacity of NLRP3 inflammasome activation. In fact, the high-level expression of the exogenous FAAH in these cells over-compensated the loss of endogenous FAAH expression, resulting in a higher level of NLRP3 after LPS priming and, correspondingly, a higher IL-1β release after Nigericin challenge, than that observed in the $FAAH^{+/+}$ BMDMs without exogenous FAAH expression (Fig. 4b, c, Fig. S6a). In contrast, expression of FAAH-S241A, a full-length FAAH variant with minimal enzymatic activity (Fig. 4a), failed to restore either NLRP3 protein expression or inflammasome activation (Fig. 4d, e), suggesting a potential role of FAAH enzymatic activity in maintaining NLRP3 stability. However, an N-terminal fragment of FAAH (aa 1–265), which had no FAAH enzymatic activity as would be expected (Fig. 4a), exhibited a comparable ability as the full-length wildtype FAAH in "rescuing" NLRP3 protein expression and IL-1β release (Fig. 4f, g), strongly arguing that FAAH enzymatic activity is not necessary for stabilizing NLRP3.

To clarify these seemingly-contradictory results, we searched for proteins that interacted with NLRP3. Unexpectedly, we found an association between NLRP3 and FAAH, as revealed by co-immunoprecipitation in LPS-primed BMDMs (Fig. 4h) and co-localization of FLAG-tagged NLRP3 with HA-tagged FAAH in HEK293T cells (Fig. S6b). Proximity Ligation Assay (PLA) further revealed a strong, intermediate and minimal NLRP3–FAAH interaction in the $FAAH^{+/+}$, $FAAH^{+/-}$, and $FAAH^{-/-}$ BMDMs (Fig. 4i). NLRP3–FAAH interaction was significantly increased at 1 h and reached a near maximum at 3 h after LPS priming, with this interaction retained upon nigericin-triggered inflammasome activation (Fig. 4j). NLRP3 was also bound to FAAH in the mouse macrophage cell line J774A.1 (Fig. S6c). The interaction between NLRP3 and FAAH was highly selective, as FAAH did not interact with other inflammasome-related proteins, including ASC, caspase-1, NEK7, NLRC4 and AIM2, and conversely, NLRP3 did not interact with monoacylglycerol lipase, another key hydrolytic enzyme in the endocannabinoid system (Fig. S6d). To gain structural insight on the NLRP3–FAAH interaction, we conducted mapping studies using HA-tagged FAAH and Flag-tagged NLRP3. Both the NACHT domain, spanning the region between aa 91 and aa 710, and the C-terminal LRR domain of NLRP3 interacted strongly with FAAH, while the N-terminal PYD domain exhibited a weak interaction with FAAH (Fig. 4k). Repeated mapping using V5-tagged NLRP3 confirmed that the PYD domain of NLRP3 interacted minimally with FAAH (Fig. S7a). Further mapping of the NACHT domain revealed the region between aa 494 and aa 710 being sufficient for NLRP3 interaction with FAAH (Fig. S7b). We also identified the region between aa 150 and aa 265 of FAAH being critically important for binding NLRP3, as the aa 1 to 265 fragment of FAAH interacted with NLRP3 while the aa 1 to 150 fragment did not (Fig. 4l). Interestingly, this region contains the entire AS sequence, a contiguous stretch of approximately 130 amino acids found in a large group of enzymes in the AS family [39]. Importantly, FAAH and FAAH (1–265) exhibited robust interaction with NLRP3, but FAAH-S241A had dramatically-reduced binding (Fig. S7c). Taken together, these results strongly suggested that the ability to interact with NLRP3, but not the enzymatic activity, was essential for FAAH to stabilize NLRP3.

Further supporting an endocannabinoids-independent role of FAAH in modulating NLRP3, 3-MA effectively inhibited autophagic degradation of NLRP3 (Fig. 3d) and restored nigericin-elicited IL-1β release (Fig. 4m) without significantly altering the level of AEA (Fig. S7d), in $FAAH^{-/-}$ BMDMs cells. In agreement, AEA did not elicit NLRP3 degradation (Fig. S7e).

FAAH also interacted with CAPS-mutated NLRP3 and anchored NLRP3 to ER and mitochondria membranes

To assess whether FAAH also interacted with CAPS-associated mutant NLRP3, we expressed HA-tagged FAAH together with one of the three FLAG-tagged mouse NLRP3 mutants (NLRP3-R258W, NLRP3-T346M and NLRP3-F521L) in 293T cells. These correspond to human NLRP3-R260W, NLRP3-T348M and NLRP3-F523L mutations found in FCAS, MWS, and NOMID patients, respectively [10]. FAAH bound to all three NLRP3 mutant proteins (Fig. 5a), suggesting that the interaction with FAAH is a common feature for CAPS-associated NLRP3 proteins. Moreover, NLRP3-R258W

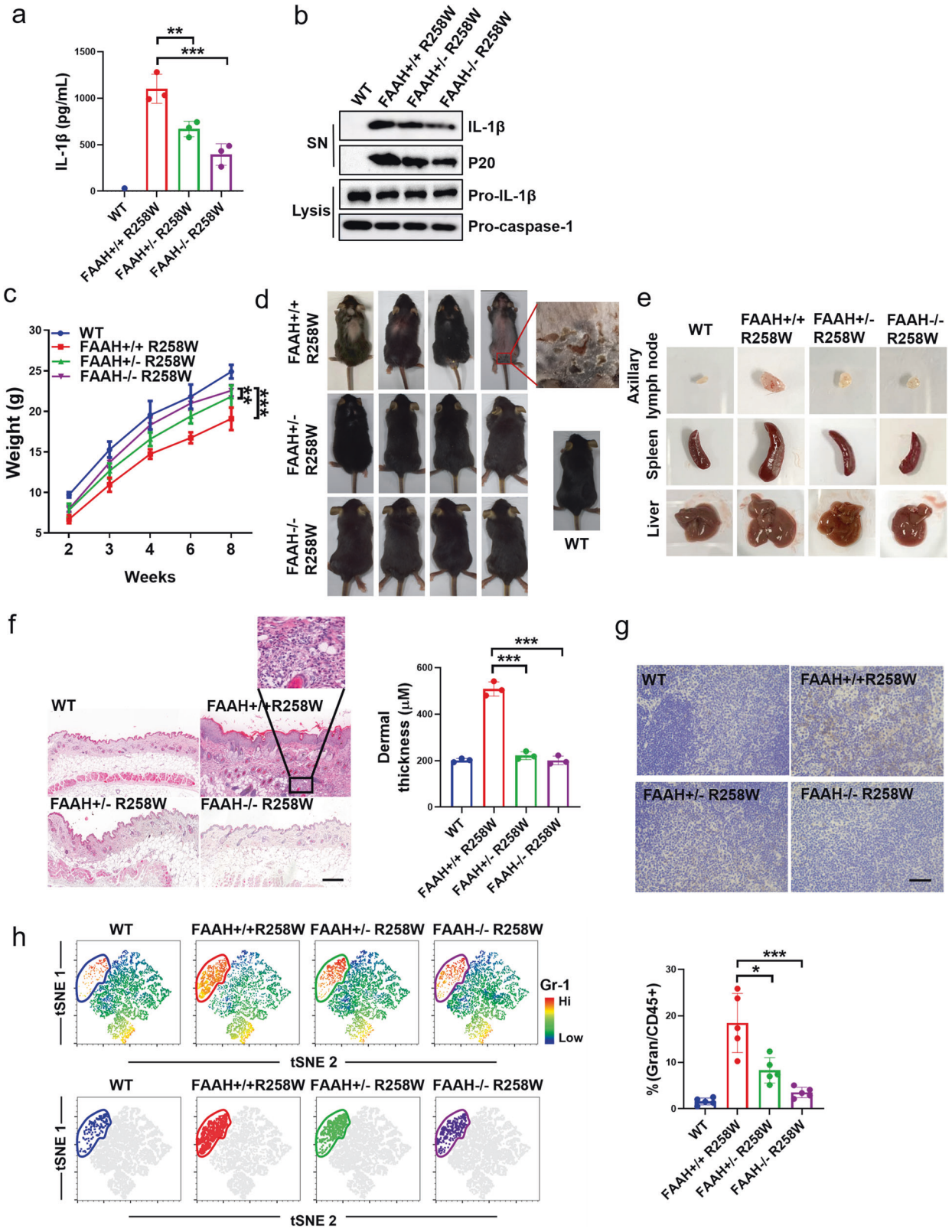

protein interacted strongly with FAAH in the *FAAH*$^{+/+}$ R258W BMDMs (Fig. 5b, c). In agreement with the reported results [14], the level of NLRP3-R258W protein was comparable to that of the wildtype NLRP3 after LPS priming, suggesting that FAAH had a similar capacity to stabilize the wildtype and mutant NLRP3 (Fig. 5d). However, heterozygous and homozygous loss of FAAH decreased NLRP3-R258W protein level by 48% and 76%, respectively, after LPS treatment (Fig. 5d).

We next assessed how FAAH affected cellular localization of NLRP3. The majority of the NLRP3 protein in *FAAH*$^{+/+}$ BMDMs was

Fig. 2 FAAH knockout inhibited the auto-inflammatory phenotype of NLRP3-R258W mice. a ELISA of IL-1β in supernatants of wildtype, $FAAH^{+/+}$ R258W, $FAAH^{+/-}$ R258W and $FAAH^{-/-}$ R258W BMDMs after LPS challenge for 3 h. Mean ± SEM, $n = 3$, $^{**}p < 0.01$; $^{***}p < 0.001$. **b** Immunoblot analysis showing IL-1β and cleaved caspase-1 (p20) in culture supernatants (SN), and Pro-caspase1 and Pro-IL-1β in the cell lysate (lysis) of wildtype, $FAAH^{+/+}$ R258W, $FAAH^{+/-}$ R258W and $FAAH^{-/-}$ R258W BMDMs following LPS challenge for 3 h. **c** Weight of wildtype, $FAAH^{+/+}$ R258W, $FAAH^{+/-}$ R258W and $FAAH^{-/-}$ R258W mice at week 2 to 8. Mean ± SD, $n = 4$ in week 8 and $n = 5$ in other weeks, using multiple comparison by two-way Anova, $^{**}p < 0.01$; $^{***}p < 0.001$. **d** Photos of wildtype, $FAAH^{+/+}$ R258W, $FAAH^{+/-}$ R258W and $FAAH^{-/-}$ R258W mice at 8 weeks. The amplified image shows inflamed skin for one of the $FAAH^{+/+}$ R258W mice. **e** Photo of the excised axillary lymph node, spleen and liver from the wildtype, $FAAH^{+/+}$ R258W, $FAAH^{+/-}$ R258W and $FAAH^{-/-}$ R258W mouse sacrificed at week 8. Similar results were obtained for mice sacrificed at week 6 (not shown). **f** H&E staining of skin section of the wildtype, $FAAH^{+/+}$ R258W, $FAAH^{+/-}$ R258W and $FAAH^{-/-}$ R258W mouse at week 8. Scale bar, 200 μm. The amplified image revealed extensive lymphocyte infiltration in the dermis of $FAAH^{+/+}$ R258W mouse but this feature was largely absent in the other mice. Right panel, quantified dermal thickness. Mean ± SEM, $n = 3$, $^{***}p < 0.001$. **g** Immunohistochemical staining of frozen sections from axillary lymph node of wildtype, $FAAH^{+/+}$ R258W, $FAAH^{+/-}$ R258W and $FAAH^{-/-}$ R258W mice using F4/80-specific antibody, revealing extensive macrophage infiltration in the $FAAH^{+/+}$ R258W mouse but much less in the other mice. Scale bar, 40 μm. **h** T-distributed stochastic neighbor embedding (t-SNE) analysis of multi-parameter flow cytometry data. See the Methods section for detail. The t-SNE algorithm was run with the normalized expression matrix by RunTSNE function in Seurat package. Right panel, the number of neutrophils relative to CD45+ cells from spleen. Mean ± SEM, $n = 3$, $^{*}p < 0.05$; $^{***}p < 0.001$.

found in the membrane fraction, which contained both ER and mitochondria, while minimal NLRP3 was observed in the cytosol fraction. However, FAAH knockout led to an increase of NLRP3 in the cytosol fraction and a corresponding decrease in the membrane fraction (Fig. 5e). Moreover, FAAH loss reduced the interaction of NLRP3 with calreticulin and TOM 20, the marker proteins for ER and mitochondria, respectively (Fig. 5f, g, h). These results demonstrated that FAAH, through physical interaction, anchored NLRP3 protein to both the ER and mitochondria membranes. FAAH also served the same anchoring role for CAPS-mutated NLRP3, as FAAH knockout dramatically reduced the association of NLRP3-R258W protein with these two organelles (Fig. 5I, j).

Select FAAH inhibitors disrupted NLRP3–FAAH interaction and induced NLRP3 degradation

A large number of FAAH inhibitors have been discovered and actively pursued as therapeutics [40, 41]. We thus conducted a preliminary study to identify FAAH inhibitors capable of reducing NLRP3 protein level. Of the 14 FAAH inhibitors we have tested, 6 of them were significantly active, as defined by the ability to reduce NLRP3 protein level by over 30% at a concentration of 40 μM (Fig. 6a). Notably, no obvious relationship was observed between the reported IC_{50} values of these compounds in inhibiting FAAH and their activity in reducing NLRP3.

URB597, one of the most active compounds in reducing NLRP3 level, was chosen for further studies. URB597 induced time-dependent NLRP3 reduction, with significant decrease observed at 3 h but not at 1 h (Fig. S8a). URB597 dose-dependently decreased NLRP3 protein level in each of the three additional cell lines we have examined, including mouse macrophage cell lines RAW264.7 and J774A.1 and human lymphoma cell line U937 (Fig. S8b–d). Furthermore, autophagy inhibitors, but not the proteasome inhibitors, abrogated the NLRP3-reducing effect of URB597 (Figs. 6b, S8e). Analogous to the scenario of FAAH loss, URB597 treatment led to enhanced K48 but not K63 ubiquitination of NLRP3 and facilitated binding of CHIP and NBR1 to NLRP3, suggesting the same selective autophagy mechanism (Fig. 6c, d). Importantly, URB597 disrupted NLRP3–FAAH interaction in BMDMs (Fig. 6e). URB597 also disrupted NLRP3–FAAH interaction in the U937 cell line (Fig. S8f), indicating a conserved mechanism by which FAAH stabilizes NLRP3 in mouse and human cells. Dopamine, on the other hand, did not disrupt NLRP3–FAAH interaction (Fig. S8g), consistent with a different NLRP3-degrading mechanism as reported previously [18]. In agreement with the results obtained under loss of FAAH, disruption of NLRP3–FAAH interaction by URB597 led to decreased binding of NLRP3 to ER and mitochondria (Fig. 6f, g, h).

Consistent with the observed NLRP3 degradation, URB597 dose-dependently inhibited inflammasome activation by Nigericin in LPS-primed BMDMs (Fig. 6i, Fig. S9a). Notably, URB597 inhibited Nigericin-triggered IL-1β release by over 90%, while FAAH knockout elicited only a 67% inhibition (Fig. 1c), suggesting that URB597 may target other pathways involved in NLRP3 inflammasome activation. In support, URB597 further reduced Nigericin-triggered IL-1β release in $FAAH^{-/-}$ BMDMs (Fig. S9b), possibly due to the ability of URB597 to restore lysosomal acidity destroyed upon inflammasome activation (Fig. S9c). URB597 also effectively blocked IL-1β release triggered by other NLRP3-specific stimuli, including ATP, MSU and Alum (Fig. S9d). Furthermore, URB597 inhibited gasdermin D cleavage, a key event of pyroptosis, induced by Nigericin (Fig. S9e). 3-MA, which abrogated the NLRP3-degrading effect of URB597 (Fig. 6b), was able to "rescue" NLRP3 inflammasome activation that was inhibited by URB597 (Fig. 6j, Fig. S9f). As 3-MA did not restore NLRP3–FAAH interaction that was disrupted by URB597 (Fig. 6e), this result indicated that the NLRP3–FAAH interaction, while being critically important for maintaining NLRP3 stability, was dispensable for NLRP3 inflammasome assembly and activation. In contrast to IL-1β release, URB597 had minimal effect on TNF-α release triggered by LPS and Nigericin challenge (Fig. S9g), suggesting a specific inhibitory effect of URB597 on NLRP3.

URB597 and PF-04457845 inhibited CAPS-associated mutant NLRP3 inflammasome activation through disrupting mutant NLRP3–FAAH interaction

Specific NLRP3 inhibitors, in particular a class of diarylsulfonylurea compounds related to MCC950, are being intensely pursued as drugs for the treatment of NLRP3-driven diseases. However, a potential caveat with these compounds is that they may be ineffective for some of the NLRP3 mutant proteins found in the CAPS patients [42]. In agreement, we found that MCC950 exhibited relatively weak activity in inhibiting LPS-elicited IL-1β release in R258W BMDMs (Fig. 7a). In contrast, both URB597 and PF-04457845, an FAAH inhibitor currently in Phase 2 clinical trials, blocked LPS-elicited IL-1β release by over 90% in these cells (Fig. 7a). Furthermore, both URB597 and PF-04457845 caused dissociation of R258W from FAAH (Fig. 7b) and decreased the level of R258W protein in a dose-dependent manner (Fig. 7c), consistent with the notion that these compounds inhibited the activation of R258W through disrupting R258W-FAAH interaction and inducing degradation of R258W protein.

To provide a preliminary indication on whether URB597 might be useful for treating CAPS patients, we isolated PBMCs from three patients, whose profiles were shown in Table 1. Interaction of CAPS-mutated NLRP3 with FAAH, and dissociation of mutant NLRP3 from FAAH upon URB597 treatment, was confirmed in the PBMCs isolated from Patient 1, a 2-year-old girl diagnosed as having FCAS with a NLRP3-A354T mutation (Fig. 7d). Compared to PBMCs isolated from her mother, who did not have CAPS, PBMCs from Patient 1 exhibited an increase in both the spontaneous and LPS-triggered release of IL-1β (Fig. 7e). URB597 was able to reduce both the spontaneous and

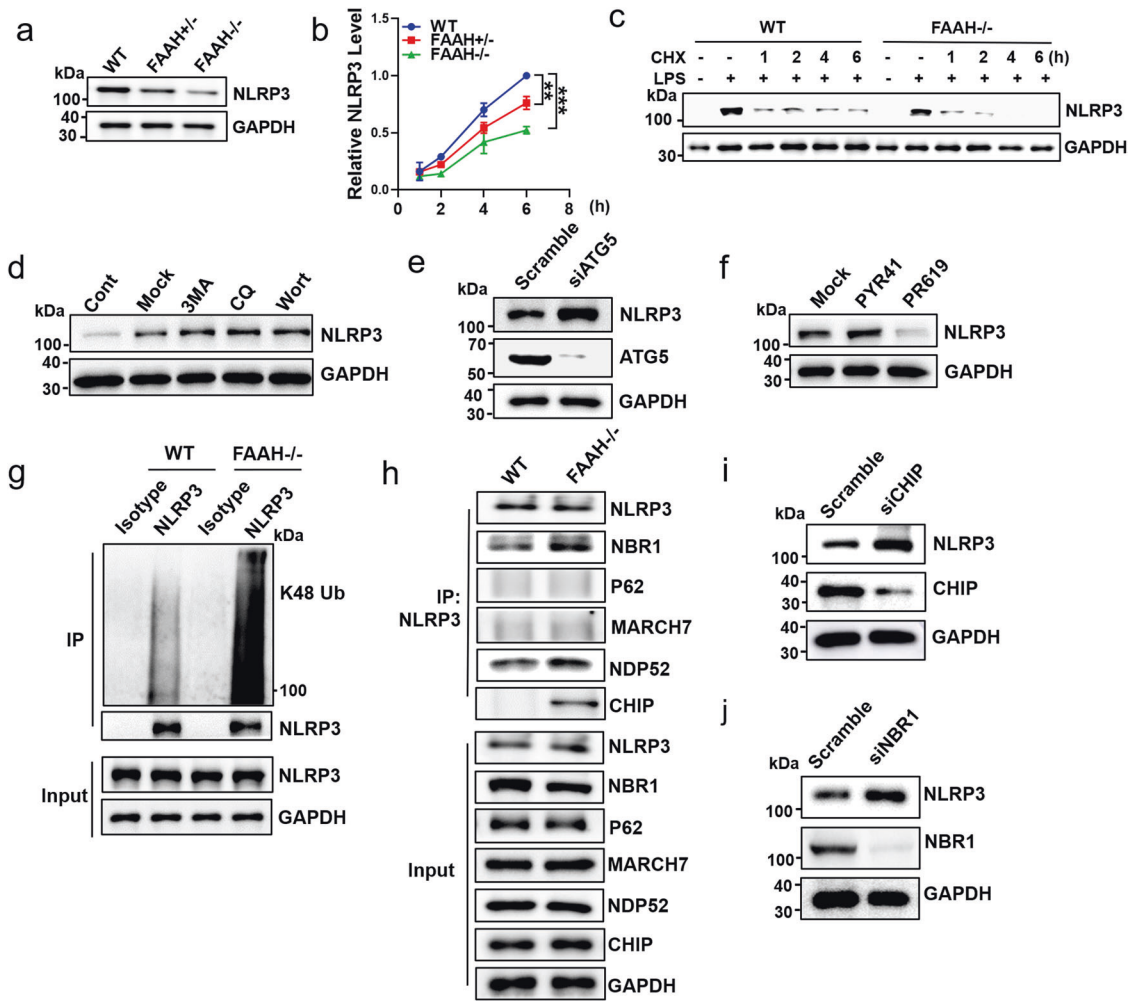

Fig. 3 NLRP3 degradation induced by FAAH loss proceeds through selective autophagy. a Immunoblot analysis of NLRP3 and GAPDH in LPS-primed BMDMs from wildtype, $FAAH^{+/-}$ and $FAAH^{-/-}$ mice. **b** NLRP3 protein level, relative to GAPDH, in wildtype, $FAAH^{+/-}$ and $FAAH^{-/-}$ BMDMs after the indicated times of LPS stimulation. The value for wildtype BMDMs treated with LPS for 6 h was set at 1.0, with the other values normalized against it. Mean ± SEM, $n = 3$. **c** Immunoblot analysis of NLRP3 and GAPDH in wildtype and $FAAH^{-/-}$ BMDMs. The cells were LPS-primed for 3 h, followed by the treatment with 10 mM of cycloheximide (CHX) for the indicated time. **d** Immunoblot analysis of NLRP3 and GAPDH in LPS-primed (Mock) $FAAH^{-/-}$ BMDMs, with or without co-treatment of 3-MA (5 mM), CQ (50 μM) or Wortmannin (1 μM). Cont, cells without LPS priming. **e** Immunoblot analysis of NLRP3 and GAPDH in LPS-primed $FAAH^{-/-}$ BMDMs that have been transfected with scrambled or ATG5-specific siRNA. **f** Immunoblot analysis of NLRP3 and GAPDH in LPS-primed (Mock) $FAAH^{-/-}$ BMDMs, with or without co-treatment of PYR41 (5 μM) or PR619 (5 μM). **g** Cell lysate of WT and $FAAH^{-/-}$ BMDMs, LPS-primed for 3 h in the presence of 3-MA (5 mM), were immunoprecipitated by a control (isotype) or NLRP3-specific antibody, followed by immunoblotting with K48-Ub or NLRP3 antibody. Input refers to unprecipitated cell lysate. **h** Cell lysate of WT and $FAAH^{-/-}$ BMDMs, LPS-primed for 3 h in the presence of 3-MA (5 mM), were immunoprecipitated with NLRP3-specific antibody, followed by immunoblot analysis of the various proteins as indicated. **i** Immunoblot analysis of NLRP3, CHIP, and GAPDH in LPS-primed $FAAH^{-/-}$ BMDMs that have been transfected with scrambled or CHIP-specific siRNA. **j** Immunoblot analysis of NLRP3, NBR1, and GAPDH in LPS-primed $FAAH^{-/-}$ BMDMs that have been transfected with scrambled or NBR1-specific siRNA.

LPS-triggered IL-1β release, while MCC950 was completely inactive. Enhanced spontaneous and LPS-triggered IL-1β release was also observed for PBMCs isolated from two other patients, a 3-year-old girl diagnosed as FCAS with a NLRP3-T350M mutation and a 7-month-old boy diagnosed as CINCA with a NLRP3-M408T mutation, respectively. URB597 again was able to inhibit both the spontaneous and LPS-triggered IL-1β release, with an inhibition rate of 55% and 65% observed on the LPS-triggered IL-1β release for Patient 2 and 3, respectively (Fig. 7f, g).

DISCUSSION

In this work we reveal a new mechanism of regulation for NLRP3 during the priming phase. We show that NLRP3 protein is inherently unstable and prone for autophagic degradation unless it is stabilized by an interaction with FAAH. In the absence of FAAH or upon dissociation of NLRP3 from FAAH, CHIP and NBR1 bind to NLRP3 and facilitates, respectively, NLRP3 ubiquitination and delivery to autophagosomes for degradation, leading to reduced NLRP3 protein level and diminished pro-inflammatory cytokine release upon inflammasome activation (Scheme 1). This process is distinct from the autophagic degradation of NLRP3 induced by dopamine [18] or p62-mediated selective autophagy triggered by NLRP3 inflammasome assembly [17]. The effect of FAAH on NLRP3 is highly specific, as FAAH does not stabilize other inflammasome sensors or other NLRP3 inflammasome components. Moreover, FAAH appears to be dispensable during the activating stage of the NLRP3 inflammasome, as the FAAH-dissociated NLRP3 protein "rescued" from autophagic degradation by 3-MA is fully competent to elicit subsequent inflammasome activation. The fact that FAAH has a

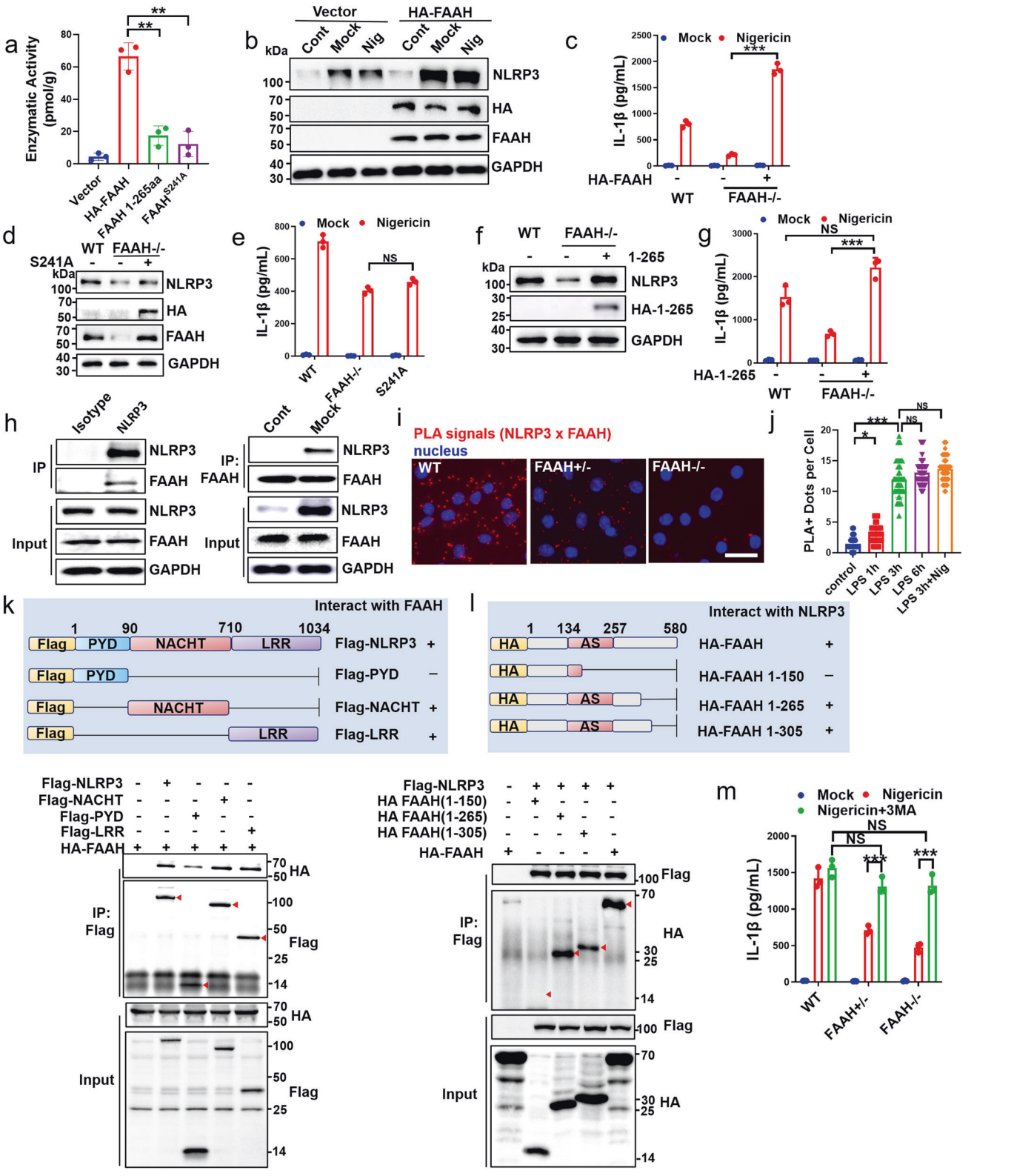

direct stabilizing role for NLRP3 also provided an explanation for the endocannabinoids-independent anti-inflammatory effect conferred by FAAH loss, as neither a CB1 nor a CB2 antagonist, nor a combination of the two agents, fully reversed the inflammation-reducing phenotype of the *FAAH*$^{-/-}$ mice in the carrageenan-induced paw edema model [43].

Our finding that FAAH served the membrane-anchoring and stabilizing role for NLRP3 is both unexpected and unsurprising. FAAH, being a rate-limiting enzyme in the endocannabinoid signaling pathway, additionally regulates NLRP3 stability. The fact that FAAH, rather than a less important protein in the endocannabinoid system, fulfills the stabilizing task for NLRP3

Fig. 4 FAAH interacted with NLRP3 and anchored NLRP3 to mitochondria and ER membranes. a The enzymatic activity of FAAH in $FAAH^{-/-}$ BMDMs, after transfection with the plasmid vector expressing HA-tagged full-length FAAH, FAAH 1–265 fragment or FAAH-S241A mutant. Transfection with the empty vector served as control. Mean ± SEM, $n = 3$. ***$p < 0.001$. **b** Immunoblot analysis using antibodies against NLRP3, HA (revealing HA-FAAH), FAAH and GAPDH in $FAAH^{-/-}$ BMDMs transfected with the vector or HA-FAAH-expressing construct. The cells were unstimulated (Cont), LPS-primed (Mock) or LPS-primed followed by Nigericin challenge (Nig). **c** ELISA of IL-1β in supernatants from non-transfected wildtype BMDMs, $FAAH^{-/-}$ BMDMs transfected with the vector and $FAAH^{-/-}$ BMDMs transfected with HA-FAAH-expressing construct. The cells were LPS-primed for 3 h (Mock) or LPS-primed followed by challenge with Nigericin for 30 min (Nigericin). Mean ± SEM, $n = 3$. ***$p < 0.001$. **d** Immunoblot analysis using antibodies against NLRP3, HA (revealing HA-FAAH), FAAH, and GAPDH in non-transfected wildtype BMDMs, $FAAH^{-/-}$ BMDMs transfected with the vector and $FAAH^{-/-}$ BMDMs transfected with HA-FAAH-S241A expressing construct. The cells were LPS-primed for 3 h. **e** ELISA of IL-1β in supernatants from non-transfected wildtype BMDMs, $FAAH^{-/-}$ BMDMs transfected with the vector and $FAAH^{-/-}$ BMDMs transfected with HA-FAAH-S241A expressing construct. The cells were LPS-primed for 3 h (Mock) and LPS-primed for 3 h followed by challenge with Nigericin for 30 min. Mean ± SEM, $n = 3$. NS non-significant. **f** Immunoblot analysis of NLRP3, HA-FAAH 1–265 and GAPDH in non-transfected wildtype BMDMs, $FAAH^{-/-}$ BMDMs transfected with the vector and $FAAH^{-/-}$ BMDMs transfected with HA-FAAH 1–265 expressing construct. The cells were LPS-primed for 3 h. **g** ELISA of IL-1β in supernatants from non-transfected wildtype BMDMs, $FAAH^{-/-}$ BMDMs transfected with the vector and $FAAH^{-/-}$ BMDMs transfected with HA-FAAH 1–265 expressing construct. The cells were LPS-primed for 3 h (Mock) and LPS-primed for 3 h followed by challenge with Nigericin for 30 min. Mean ± SEM, $n = 3$. ***$p < 0.001$. **h** Left panel, cell lysate of LPS-primed BMDMs were immunoprecipitated with isotype or NLRP3-specific antibody followed by immunoblot analysis of NLRP3 and FAAH. Right panel, cell lysate of untreated (Cont) or LPS-primed (Mock) BMDMs were immunoprecipitated with FAAH-specific antibody followed by immunoblot analysis of NLRP3 and FAAH. **i** PLA of NLRP3–FAAH interaction in LPS-primed wildtype, $FAAH^{+/-}$ and $FAAH^{-/-}$ BMDMs. Scale bar, 20 μm. **j** Number of PLA-positive dots for NLRP3–FAAH interaction in wildtype BMDMs after LPS priming for the indicated time or LPS-primed for 3 h followed by Nigericin challenge for 30 min. 50 cells were counted for each treatment. Mean ± SEM. **k**, **l** Flag-tagged NLRP3 constructs and HA-tagged FAAH constructs were co-expressed in HEK293T cells. Immunoblot analysis of HA and Flag proteins in cell lysates immunoprecipitated with anti-Flag antibody. **m** ELISA of IL-1β in supernatants of wildtype, $FAAH^{+/-}$ and $FAAH^{-/-}$ BMDMs that were LPS-primed (Mock), LPS-primed followed by Nigericin challenge (Nigericin), or LPS-primed in the presence of 3-MA followed by Nigericin challenge (Nigericin + 3-MA). Mean ± SEM, $n = 3$. ***$p < 0.001$. NS non-significant.

is intriguing. It raises the question whether the observed NLRP3–FAAH interaction could be a two-way cross-talk, with NLRP3 also playing a regulatory role on the function of FAAH. On the other hand, the membrane-anchoring role of FAAH would not be surprising. FAAH is known for its various intracellular membrane localizations including mitochondria, ER and Golgi, all of which have been reported as the intracellular destinations of NLRP3. Compared to the other membrane-anchoring molecules identified so far, FAAH, being an unanimously-expressed membrane protein, is better positioned to serve a general-purpose anchoring function for NLRP3.

As NLRP3 is a node for immune sensing and underpins a broad spectrum of diseases associated with lifestyle and ageing, direct targeting of NLRP3 holds tremendous therapeutic potential. Compounds that can inhibit NLRP3 inflammasome assembly and activation, and to a lesser degree, that can adversely affect NLRP3 priming, are being intensively pursued. Our work suggested a novel strategy for NLRP3 drug development, through inducing NLRP3 degradation via disrupting NLRP3–FAAH interaction. This strategy is advantageous as it applies equally well for both wild-type and CAPS-mutated NLRP3. Our work, based on a small number of compounds, have identified several FAAH inhibitors with the ability to induce dissociation of NLRP3 from FAAH and subsequent NLRP3 degradation. Further screening of a larger pool of existing FAAH inhibitors should yield compounds with better NLRP3-degrading capability. Moreover, agents that can specifically disrupt NLRP3–FAAH interaction without inhibiting FAAH would be highly desirable, as they may exert therapeutic benefits without the potential toxicities associated with the inhibition of FAAH enzymatic activity.

METHODS

Chemical compounds

URB597 (10046), Arachidonoyl Ethanolamide (90050) were purchased from Cayman Chemical (USA). JNJ-42165279 (S0497), MG-132(S2619), PS-341/Bortezomib(S1013), b-AP15(S4920) were purchased from Selleck (USA). PF-04457845 (HY-14376), JZL195 (HY-15250), LY2183240 (HY-10865), PF-3845 (HY-14380), Biochanin A (HY-14595), N-Benzyllinolenamide (HY-N3033), Carprofen (HY-B1227), BIA10-2474 (HY-19740), FAAH-IN-2 (HY-79511), N-Benzylpalmitamide (HY-N2365), 1-monomyristin (HY-N2512), SA 47 (HY-18080), 3-Methyladenine (HY-17394), Chloroquine (HY-17589), Wortmannin (HY-10197), PYR-41 (HY-13296), PR-619 (HY-13814), Cycloheximide (HY-112951), MCC950 (HY-12815A) were purchased from MedChemExpress (USA). Dopamine hydrochloride (H8502) was purchased from Sigma-Aldrich (USA).

Antibodies

The primary antibodies were anti-NLRP3: CST (1510S) and Adipogen (AG-20B-0014-C100); anti-FAAH1: Abcam (ab54615), CST (2942S), Affinity (DF6308) and Proteintech (17909-I-AP); anti-IL-1β (R&D, AF-401-NA), anti-caspase-1 (Adipogen, AG-20B-0042-C100), anti-ASC/TMS1 (CST, 67824S), anti-Nek7 (Santa Cruz, sc-398439), anti-k48-Ub (CST, 12805S), anti-k63-Ub (eBioscience, 14-6077-82), anti-CHIP (Santa Cruz, sc-133066), anti-NBR1 (CST, 9891S), anti-NDP52 (CST, 60732S), anti-MARCH7 (Prosci, 25-847), anti-LC3B (NOVUS, NB100-2220), anti-P62 (Santa Cruz, sc-48402), anti-NLRC4/CARD12 (Abcam, ab201792), anti-AIM2 (Abcam, ab180665), anti-HA (Proteintech, 66006-I-Ig), anti-Flag (Proteintech, 20543-1-AP), anti-V5 (Proteintech, 14440-1-AP), anti-Tom20 (CST, 42406S), anti-GSDMD (Abcam, ab209845), anti-ATG5 (CST, 12994), anti-Calreticulin (CST, 12238S), anti-NF-κB (CST, 8242T), anti-Phospho-NF-κB (Ser536) (CST, 3033T), anti-IκBα (CST, 4814T), anti-Phospho-IκBα (Ser32) (CST, 2859T), anti-F4/80 (CST, 70076S), anti-GAPDH (Affinity, AF7021), anti-β-actin (Proteintech, 66009-I-Ig). Secondary antibodies were anti-Mouse IgG HRP conjugate (Promega, W402B), anti-Rabbit IgG HRP conjugate (Promega, W401B) and anti-Goat IgG HRP conjugate (Promega, V805A).

Mice

C57BL/6 mice were originally purchased from Jackson Laboratories and maintained in our facility. The $FAAH^{-/-}$ mice (ko-1 and ko-2) on C57BL/6 background were separately created by GemPharmatech (http://order.gempharmatech.com/strain/index?quick_search=&keyword_type=1&keyword=FAAH&strain_id=17633&paging=, Jiang Shu, China) and Cyagen (https://www.cyagen.com/cn/zh-cn/sperm-bank/14073, Shu Zhou, China), using CRISPR-Cas9 technology. $NLRP3^{R258W}$ mice were originally purchased from Jackson Laboratories (gifted from Dr. Warren Strober, NIH). All animals received care in compliance with the guidelines outlined in the Guide for the Care and Use of Laboratory Animals and maintained at the SPF animal facility. $FAAH^{-/-}$ were crossed with $NLRP3^{R258W}$ mice to obtain R258W $FAAH^{+/-}$ mice, and R258W $FAAH^{+/-}$ mice were further crossed with $FAAH^{-/-}$ mice to obtain R258W $FAAH^{-/-}$ mice.

Cell lines

HEK293T, J774A.1, RAW264.7, U937, and L929 cell lines were purchased from ATCC. The cell lines tested negative for mycoplasma contamination. HEK293T, J774A.1, RAW264.7, and L929 cells were cultured in DMEM supplemented with 10% FBS and 10% penicillin and streptomycin. U937 were cultured in RPMI 1640 containing the same supplements.

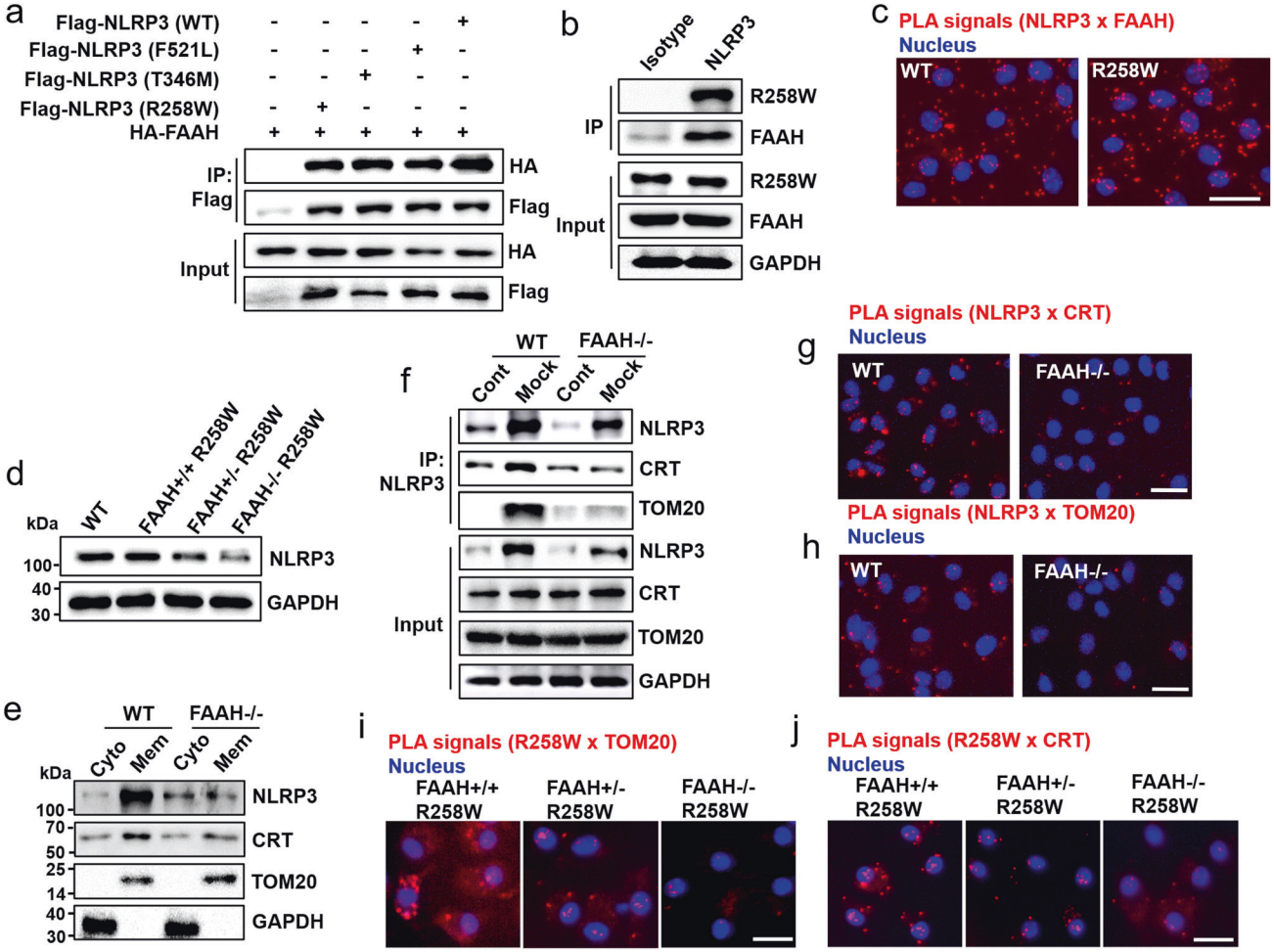

Fig. 5 FAAH interacted with CAPS-mutated NLRP3 and anchored NLRP3 to ER and mitochondria membranes. a Lysates of HEK293T cells, after co-transfection with HA-FAAH construct and wild-type Flag-NLRP3 or one of the three mutant Flag-NLRP3 constructs, were immunoprecipitated with anti-Flag antibody followed by immunoblot analysis of HA and Flag proteins. **b** Cell lysate of LPS-primed NLRP3-R258W BMDMs were immunoprecipitated with isotype or NLRP3-specific antibody, followed by immunoblot analysis of NLRP3-R258W and FAAH. **c** PLA of NLRP3–FAAH interaction in LPS-primed wildtype NLRP3 and NLRP3-R258W BMDMs. Scale bar, 20 μm. **d** Immunoblot analysis of NLRP3 and GAPDH in LPS-primed BMDMs derived from wildtype, *FAAH*$^{+/+}$ R258W, *FAAH*$^{+/-}$ R258W, and *FAAH*$^{-/-}$ R258W mice. **e** Immunoblot analysis of NLRP3, CRT, TOM20 and GAPDH of the cytosol (Cyto) and membrane (Mem) fraction of cell lysates in LPS-primed wildtype and *FAAH*$^{-/-}$ BMDMs. **f** Cell lysates of wildtype and *FAAH*$^{-/-}$ BMDMs were immunoprecipitated with anti-NLRP3 antibody followed by immunoblot analysis of NLRP3, CRT and TOM20. The cells were either unstimulated (Cont) or LPS-primed for 3 h (Mock). **g**, **h** PLA of NLRP3 interaction with CRT (**g**) and TOM20 (**h**) in LPS-primed wildtype and *FAAH*$^{-/-}$ BMDMs. Scale bar, 20 μm. **I**, **j** PLA of NLRP3-R258W interactions with TOM20 (**i**) or CRT (**j**) in LPS-primed *FAAH*$^{+/+}$ R258W, *FAAH*$^{+/-}$ R258W, and *FAAH*$^{-/-}$ R258W BMDMs. Scale bar, 20 μm.

Immunoblotting analysis

Washed BMDMs with PBS, lysed the cells in RIPA buffer containing SDS and β-mercaptoethanol, and added protease inhibitor 1% cocktail (Sangon Biotech, C600386). Then loaded the cell lysate containing 10–20 μg protein on a 13.5% polyacrylamide gel, performed electrophoretic separation, and transferred it to a nitrocellulose (NC) membrane. The membrane was blocked in 5% skimmed milk 30 min. Incubated with primary antibody overnight at 4 °C. The next day, secondary horseradish peroxidase (HRP) binding antibody was incubated for 2 h at room temperature and detected by GE Amersham Imager 600 imaging system.

Isolation and culture of BMDMs

The mice aged about 8 weeks were killed by cervical dislocation. The hind legs were cut off, the muscles were removed, the leg bones were clamped with forceps, and the joints at both ends were cut off. DMEM medium (Gibco, 12800082) was absorbed with a syringe, and then inserted into the leg bones to remove the marrow cell, centrifuged at 1500 rpm for 5 min, collected the cell pellet, added 1 mL red cell lysis solution (Biosharp, BL503B) for 2 min, and added 3 mL DMEM medium, centrifuged at 1500 rpm for 5 min. Primary BMDMs were cultured for 4 days in DMEM supplemented with 10% fetal bovine serum (Biological Industries, 04-001-1ACS), 25% supernatant of L929 cells (L929 cells were cultured with DMEM and the supernatant was collected and filtered with 0.22μm membrane filter), and 10% Penicillin–Streptomycin solution (HyClone, SV30010).

Stimulation of BMDMs

3×10^5 BMDMs were plated in 24-well plate overnight and the medium was changed to Opti-MEM in the following morning, and then was primed with 100 ng/mL ultra-pure LPS (Escherichia coli 055: B5, Sigma-Aldrich, L6529), typically for 3 h, followed by challenge with 5 μM Nigericin (Sangon Biotech, A60668) for 30 min, 2.5 mM ATP (Sangon Biotech, A600311) for 30 min or 150 μg/mL MSU (Invitrogen, tlrl-msu) for 6 h or 300 μg/mL Alum (Thermo, 77161) for 6 h. The procedures for various inhibitor treatments are described in the figure legends.

AIM2 and NLRC4 inflammasome activation

3×10^5 BMDMs were plated in 24-well plate overnight and the medium was changed to Opti-MEM in the following morning, and then was primed with 100 ng/mL ultra-pure LPS (Escherichia coli 055: B5, Sigma-Aldrich, L6529) for 3 h. for AIM2 inflammasome activation, 1 μg/mL Poly(dA:dT) was

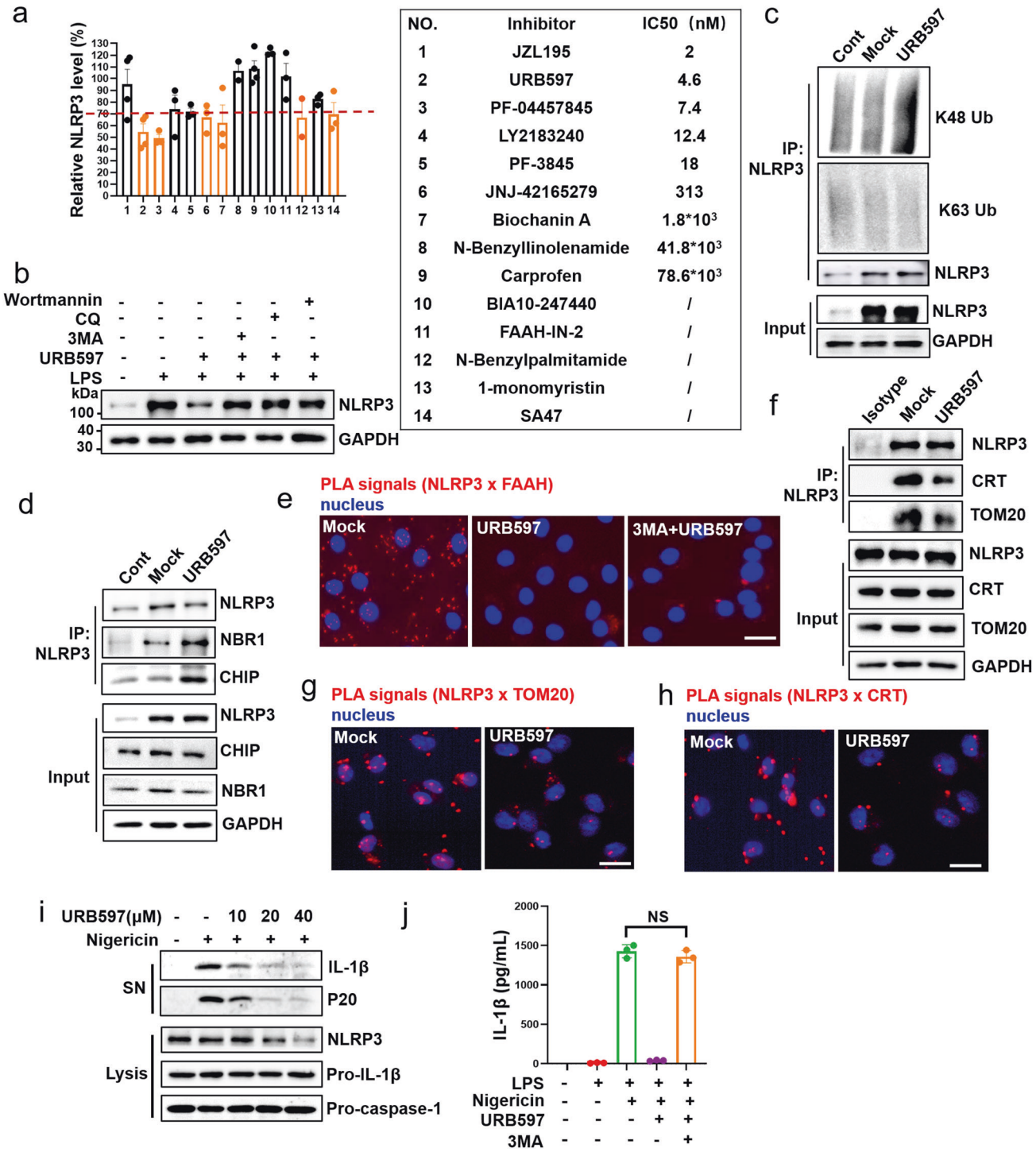

NO.	Inhibitor	IC50 (nM)
1	JZL195	2
2	URB597	4.6
3	PF-04457845	7.4
4	LY2183240	12.4
5	PF-3845	18
6	JNJ-42165279	313
7	Biochanin A	$1.8*10^3$
8	N-Benzyllinolenamide	$41.8*10^3$
9	Carprofen	$78.6*10^3$
10	BIA10-247440	/
11	FAAH-IN-2	/
12	N-Benzylpalmitamide	/
13	1-monomyristin	/
14	SA47	/

transfected with 0.75 μL Lipofectamine 3000 (Thermo Fisher: L3000-15) for 4 h. For NLRC4 inflammasome activation, a single colony of Salmonella typhimurium strain ST 1433 strain was grown in antibiotic-free Luria Bertani (LB) media until OD_{450} reached 0.5- 0.6. Prior to infection, Salmonella resuspended in 1 mL sterile PBS. BMDMs were infected at multiplicity of infection (MOI) of 10:1 (bacteria: cells) for 30 mins, then washed with PBS and cultured cells with Opti-medium containing 50 μg/mL Gentamicin (Sangon NO. A620217) for 4 h.

shRNA Mediated Gene knockdown in BMDMs

The PLVX-shRNA Lentiviruses vector was purchased from YouBio, Lentiviral PLVX- shRNA targeting FAAH constructs were generated in the same vector background using Gibson assembly. PLVX-shRNA scramble was used as a negative control. Lentiviruses were packaged in HEK293T cells using packaging plasmids pMD2.G and psPAX2 in DMEM supplemented with 10% FBS. The supernatant of Lentiviruses was collected 48 and 72 h after transfection, concentrated by Lenti-X concentrator and stored at −80 °C. After cultured BMDMs for 3 days, transduced 5 ml supernatant with lentivirus containing PLVX-shFAAH for 6 h, then added 5 ml fresh DMEM and cultured for the other 2 days and changed the fresh DMEM. The fifth day, plated the BMDMs in 24-well plates. Knockdown efficiency was analyzed by immunoblotting with antibody against FAAH. FAAH shRNA: CCGGGCATTGTGCATGAAAGCCCTACTCGAGTAGGGCTTTCATGCACAATGCTTTTTG.

Fig. 6 URB597 disrupted NLRP3–FAAH interaction and induced NLRP3 degradation. a NLRP3 protein level in BMDMs, after LPS priming for 3 h followed by the treatment of the indicated FAAH inhibitors (40 μM) for another 3 h, was analyzed by immunoblotting and quantified by Image J. NLRP3 protein level, relative to GADPH, was normalized against the NLRP3 protein level in the cells primed with LPS for 3 h followed by DMSO treatment for another 3 h. Mean ± SEM, $n = 3$. IC50 values (for inhibiting FAAH activity) were taken from www.cayman.com, www.SelleckChem.cn or www.MedChemExpress.com. **b** Immunoblot analysis of NLRP3 and GAPDH in BMDMs after the indicated treatment. Cells were LPS-primed for 3 h followed by DMSO (Mock) or URB597 treatment for another 3 h in the presence or absence of autophagy inhibitors. Dosing: 3-MA; 5 mM; CQ, 50 μM; Wortmannin, 1 μM; URB597, 40 μM. **c** Cell lysates from BMDMs were immunoprecipitated by an NLRP3-specific antibody, followed by immunoblotting with K48-Ub, K63-Ub or NLRP3 antibody. The cells were unstimulated (Cont), LPS-primed for 3 h followed by DMSO (Mock) or URB597 (40 μM) treatment for 1 h. **d** Cell lysates from BMDMs were immunoprecipitated by an NLRP3-specific antibody, followed by immunoblotting with NLRP3, NBR1, and CHIP antibody. The cells were unstimulated (Cont), LPS-primed for 3 h followed by DMSO (Mock) or URB597 (40 μM) treatment for 1h. **e** PLA of NLRP3–FAAH interaction in mouse BMDMs that were LPS-primed for 3 h, followed by the treatment of DMSO (Mock), URB597 or URB597 plus 3-MA for 1 h. Scale bar, 20 μm. **f** Cell lysate of mouse BMDMs that were LPS-primed for 3 h, followed by the treatment of DMSO (Mock) or URB597 for 1 h, were immunoprecipitated with isotype or NLRP3-specific antibody, followed by immunoblot analysis of NLRP3, CRT and TOM20. **g**, **h** PLA of NLRP3 interaction with TOM20 (**g**) or CRT (**h**) in mouse BMDMs that were LPS-primed for 3 h followed by DMSO (Mock) or URB597 treatment for 1 h. Scale bar, 20 μm. **i** Immunoblot analysis of IL-1β and cleaved caspase-1 (p20) in culture supernatants (SN) and pro-caspase-1 and pro-IL-1β in the cell lysates (lysis). BMDMs were LPS-primed for 3 h, then treated with indicated concentrations of URB597 for another 3 h, followed by Nigericin challenge for 30 min. **j** ELISA of IL-1β in supernatants of BMDMs. After LPS priming for 3 h, the cells were treated with URB597 for another 3 h in the presence or absence of 3-MA, followed by Nigericin challenge for 30 min. Mean ± SEM, $n = 3$. NS non-significant.

Genotype identification of knockout mice

The genotype of knockout mice was identified by PCR followed by sequencing. The toes of the mice were cut off, and the mice were numbered by cutting the toes. First, the toe tissue was dissolved in 50 mM NaOH and placed in a sample cooker and heated for 30 min at 100 °C. At the end of pyrolysis, 1 M Tris-HCl was added to neutralize the solution to pH 7.0. The tissue fragments were removed after centrifugation at 3000 g for 5 min. The supernatant containing DNA was used for PCR experiments. After PCR, 1 × TAE gel with 1% agarose was prepared for electrophoresis separation. Four primer pairs were used for $FAAH^{-/-}$ mice from GemPharmatech (ko-1): KO: GTTGGATCTGGTAACGGGGGA and CATTTGC TGGGTCTCCCGCTAG, located in exon 2 through exon 15 and generating a fragment of 542 bp; WT 1: CAGAGGGGCCTGAGGGC and CATTTGCTGGG TCTCCCGCTAA, located in exon 15 and generating a fragment of 527 bp; WT 2: CATGCTTCTGGTTACCCTTTC and GAAAGAAGACAGCGACAATGC, located in exon 3 and generating a fragment of 333 bp; WT 3: TCAGAAATGAGAGAAGGTAATGGG and GGGTAACACATTACGTCAATCTAGC, located in exon 2 and generating a fragment of 506 bp; Two primer pairs were used for the $FAAH^{-/-}$ mice from Cyagen (ko-2): WT: TCAGAAATGAGA GAAGGTAATGGG and GGGTAACACATTACGTCAATCTAGC, located in exon 2 and generating a fragment of 506 bp; KO: TCAGAAATGAGAGAAGGTAA TGGG and AAGTAGCCTTTGTAGTGTTCCATCT, located in exon 2 through 13 and generating a fragment of 598 bp; The primers for the NLRP3 (R258W) mice: CCATGAGTTCCCTTAAGCTGG and GGCTGCTTAGCAGAATGTCTC, located in exon 3 and generating a fragment of 333 bp.

MSU-induced peritonitis

MSU-induced peritonitis was induced by intraperitoneal injection of 50 mg/kg MSU crystals. After 6 h, mice were sacrificed by exposure to CO_2 and peritoneal cavities were washed with 10 ml cold PBS. Neutrophil infiltration in peritoneal lavage fluid was assessed by flow cytometry using the neutrophil markers Ly6G and CD11b and expressed as the number of neutrophils per 10^7 cells in the peritoneal cavity. Serum IL-1beta was determined by ELISA.

LDH release assay

Lactate dehydrogenase release from cultured cells was measured according to the LDH Cytotoxicity Assay Kit, following manufacturer's instructions (Beyotime, Product #: C0016). Biotek Cytation5 was used to detect the signals at 490 nm.

Elisa

Serum or supernatants of cell culture were assayed for mouse IL-1β (R&D Systems, DY401), mouse TNF-α (R&D Systems, DY201), mouse IL-18 (MBL, 7625) or human IL-1β (R&D Systems, DLB50) according to the manufacturer's instructions. Biotek Cytation5 was used to detect the signals at 450 nm.

siRNA mediated gene knockdown in BMDMs

After culturing BMDMs for 3 days, cells were transfected with 50 nM siRNA using Lipofectamine RNAi MAX (Invitrogen, 13778150) according to the manufacturer's guidelines. ATG5 siRNA: 5′-CUCUAUCAGGAUGAGAUAA TT-3′; CHIP siRNA: CCCUGUGCUAUCUGAAGAUTT; NBR1 siRNA: GGAGAUU GUCCACAUUGUUTT; NDP52 siRNA: GGUUGUUAUCAAUAAGGAATT.

Proximity ligation assay

The cells were cultured on 96-well plate and fixed by 4% PFA. PLA assay was performed according to manufacturer's instruction (Duolink® PLA kit, Sigma-Aldrich, DUO92101). Nucleus was revealed in blue in the images (Nucleus were stained using Duolink® In Situ Mounting Medium with DAPI.). Images were acquired on Nikon TI inverted Fluorescence microscope (Nikon, TI-DH, Japan) and analyzed using the vendor software.

Lysosome acidification study

3×10^5 BMDMs were plated in 24-well plate overnight and the medium was changed to Opti-MEM in the following morning, and then was primed with 100 ng/mL ultra-pure LPS (Escherichia coli 055: B5, Sigma-Aldrich, L6529) for 3 h, then URB597 treated for 3 h, followed by challenge with 5 μM Nigericin (Sangon Biotech, A60668) for 30 min. Washed cells and incubated cells with HBSS containing 50 nM Lysotracker Green (Beyotime, C1047S) for 30 mins. Images were acquired on Nikon TI inverted Fluorescence microscope (Nikon, TI-DH, Japan) and analyzed using the vendor software.

FAAH enzyme activity determination

The brain tissue of the mouse was taken out, and the lysate was added to prepare a protein suspension; for the FAAH enzyme activity of BMDMs cells, the collected cells were lysed on ice with vortex, then centrifuged at 300 × *g*, 5 min, 4 °C and the protein concentration was detected with a BCA quantitative kit (Beyotime, China, www.beyotime.com; Product #: P0012S). The FAAH enzyme activity was determined by using a commercial kit (GENMED SCIENTIFICS INC.U.S.A, Catalog #: GMS50737.1 V.A), following the manufacturer's instructions [44].

AEA assay

The brain tissue of the mouse was taken out and ground under liquid nitrogen, followed by the addition of pre-cooled chloroform and methanol (chloroform: methanol: sample volume ratio was 4:2:1) and shaking at the bench-top vibrator to avoid emulsification. After centrifugation at 800 × *g* for 15 min at 4 °C, withdrew all the organic phase liquid (lower liquid phase) and blew dry in Nitrogen; added pre-cooled absolute ethanol and ddH_2O, used HCl to correct pH = 3.0. Used methanol to activate the C-18 Sep-Pak solid phase extraction column in advance, connected the negative pressure system at the bottom of the extraction column; added the above sample solution to the extraction column, and used 10% ethanol after adsorption to rinse the extraction column, and finally acetonitrile/ethyl acetate solution (volume ratio 1:1) was added to the extraction column for elution; collected the eluent, blew dry in nitrogen, added 1 mL of n-hexane to dissolve, and detected by GC-MS instrument.

Hypothermal response experiment

Surface temperature was determined by infrared camera. The pre-injection surface temperature for WT mice (34 °C ± 0.2 °C) and $FAAH^{-/-}$ mice

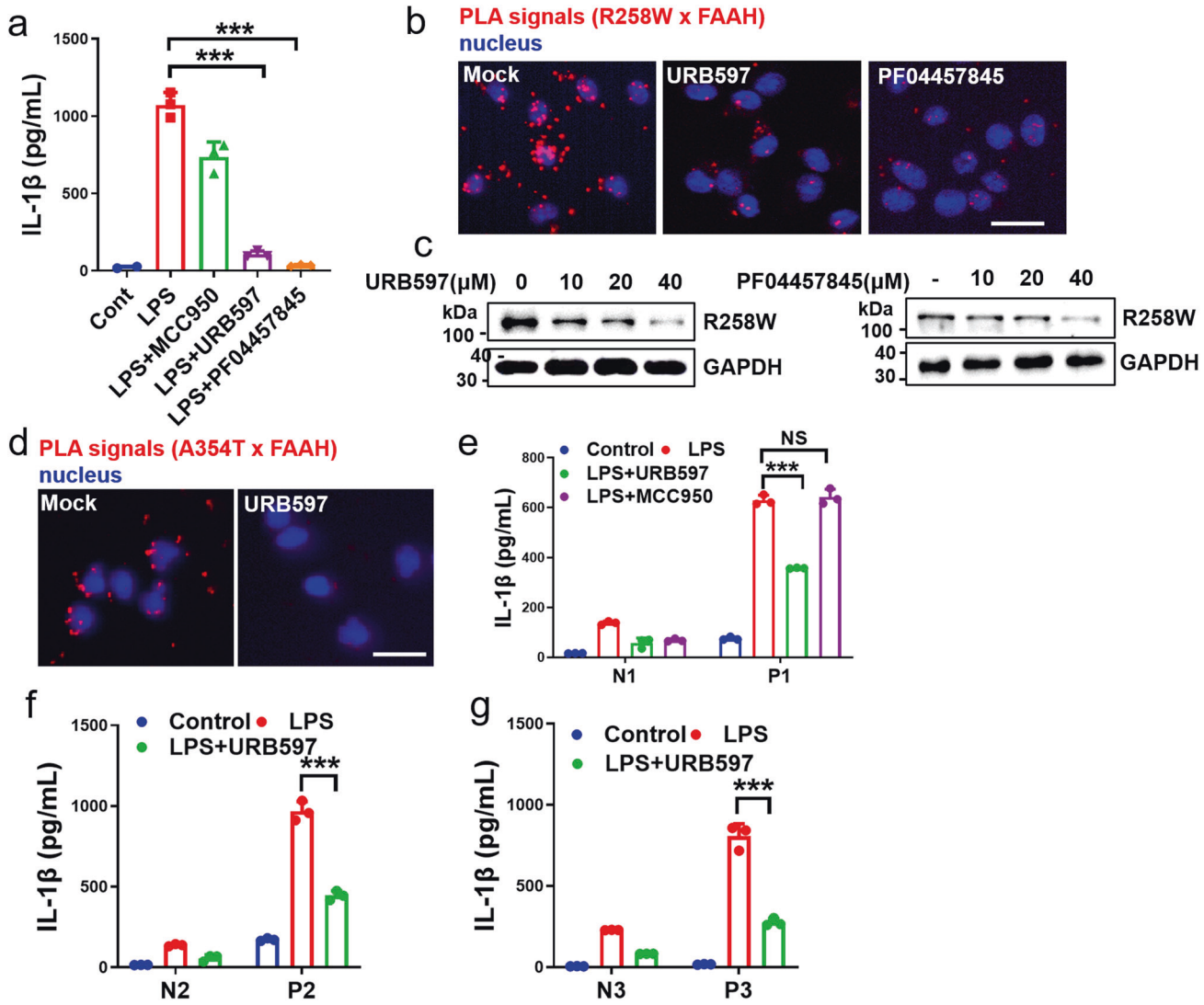

Fig. 7 URB597 and PF-04457845 inhibited CAPS-associated mutant NLRP3 inflammasome activation through disrupting mutant NLRP3–FAAH interaction. a ELISA of IL-1β in supernatants of NLRP3-R258W BMDMs that were untreated (Cont), treated with LPS for 4 h, and treated with LPS for 4 h in the presence of MCC950 (10 mM) or URB597 (40 μM) or PF-04457845 (40 μM). Mean ± SEM, $n = 3$, ***$p < 0.001$. **b** PLA of NLRP3–FAAH interaction in NLRP3-R258W BMDMs treated with LPS for 3 h followed with PBS (Mock), URB597 or PF04457845 treatment for 1 h. Scale bar, 20 μm. **c** Immunoblot analysis of NLRP3 and GAPDH in NLRP3-R258W BMDMs that were LPS-treated for 3 h, followed by treatment with different doses of URB597 or PF04457845 for another 3 h. **d** PLA of NLRP3–FAAH interaction in PBMCs from Patient 1. The cells were treated with LPS for 3 h followed by DMSO (Mock) or URB597 (40 μM) treatment for 1 h. Scale bar, 20 μm. **e** ELISA of IL-1β in supernatants of PBMCs isolated from Patient 1 and her normal mother. The cells were untreated (Cont) or treated with LPS, LPS plus URB597 (40 μM) or LPS plus MCC950 (10 mM) for 4 h. Mean ± SEM, $n = 3$, ***$p < 0.001$. NS non-significant. **f**, **g** ELISA of IL-1β in supernatants of PBMCs isolated from Patient 2 (**f**) and 3 (**g**). The cells were untreated (Cont), treated with LPS or LPS plus URB597 (40 μM) for 4 h. Mean ± SEM, $n = 3$, ***$p < 0.001$. N2 was Patient 2's normal mother, while N3 was an unrelated normal boy. Mean ± SEM, $n = 3$, ***$p < 0.001$.

(34 °C ± 0.2 °C) mice were equivalent. Surface temperature were assessed at 60 min post-injection unless otherwise stated. Mice were injected intraperitoneally of Arachidonoyl Ethanolamide at a dose of 5 mg/kg, 12.5 mg/kg, 25 mg/kg and 50 mg/kg Arachidonoyl Ethanolamide, respectively. Recorded temperature and analyzed data by Thermal Imaging System for Infrared Camera [36].

Pain sensitivity experiment

6-week-old WT mice and *FAAH*$^{-/-}$ mice were used. In the tail swinging experiment, when the mice were not injected with anything, the time of mouse was hand-held with 1 cm of the tip of the tail immersed into a water bath maintained at 56.0 °C and the latency for the animal to withdraw its tail was scored, then mice were injected intraperitoneally of Arachidonoyl Ethanolamide (Cayman chem, 90050) at a dose of 50 mg/kg, 5 min later. Nociception was then assessed in the tail immersion assay, where each mouse was hand-held with 1 cm of the tip of the tail immersed into a water bath maintained at 56.0 °C and the latency for the animal to withdraw its tail was scored. In the hot plate experiment, mice were injected intraperitoneally of Arachidonoyl Ethanolamide at a dose of 50 mg/kg, after 5 min, the mice were placed on a hot plate at 56 °C, and the time of climbing out of the hot plate was recorded [36].

Real-time PCR assays

RNA was extracted from the cells using RNAiso Plus (TaKaRa, 9108/9109) and the mRNA expression level was measured by quantitative RT-PCR using FastStart Essential DNA Green Master (Roche, 4147400) according to the manufacturer's instructions at a final volume of 20 μL. The gene expression level of NLRP3 was normalized with GAPDH, and the average was presented with standard deviation from duplicates or triplicates of repeated experiments. Real-Time PCR primers were designed by Primer Premier 5.0. The following cycling program was used for SYBR green assay: initial denaturation at 95 °C for 10 min; 40 cycles of 95 °C for 15 s and 60 °C

Table 1. The Blood Routine of three CAPS patients.

Items	P1	P2	P3	Reference	Unit
C-reactive protein, CRP	68	49	96	<8	mg/L
White blood cells, WBC	31.7	13.1	20.0	4.0–10.0	10^9/L
neutrophilic granulocyte, NEUT#	23.0	8.5	8.4	0.7–4.6	10^9/L
lymphocyte, LYMPH#	8.0	3.8	10.0	1.48–7.8	10^9/L
hemoglobin, Hgb	89	90	81	110–160	g/L
Platelets, Plt	824	579	558	100–400	10^9/L
Erythrocyte sedimentation rate, ESR	22	46	40	0–20	mm/h

for 60 s; followed by a melt curve step. mRNA expression profiles were normalized to levels of housekeeping gene Glyceraldehyde 3-phosphate dehydrogenase (GAPDH) in each sample and the fold-change in expression was calculated by the $2^{-\Delta\Delta Ct}$ method by The LightCycler® 96 System. Real-Time PCR primers were designed by Primer Premier 5.0 and their sequences were as follows: 1. GAPDH-F: TGGATTTGGACGCATTGGTC; R: TTTGCACTGGTACGTGTTGAT. 2. NLRP3-F: ATTACCCGCCCGAGAAAGG; R: TCGCAGCAAAGATCCACACAG.

Co-immunoprecipitation

For immunoprecipitation, BMDMs were lysed in NP-40 lysis buffer (1% NP-40, 150 mM NaCl, 50 mM HEPES), and lysates were cleared by centrifugation at maximum speed for 15 min. Whole-cell lysates were incubated with 1 μg of the indicated primary antibodies on a rocking platform for 2–4 h at 4 °C. Protein A/G PLUS-Agarose (Santa Cruz) beads were washed, incubated for 30 min with 3% BSA and then added to the samples. Incubation was continued for an additional 12 h on the rocking platform at 4 °C. The agarose beads were collected by centrifugation and washed six times with the NP-40 lysis buffer. After washes, immunoprecipitates were eluted in sample buffer and used for immunoblotting analysis.

Mapping studies

The PCDNA3.1-FAAH-3x HA expression clone was purchased from Sino Biological. PCDNA3.1-3x HA-FAAH 1-150 (residues 1-150), PCDNA3.1-3x HA-FAAH 1–265 (residues 1–265) and PCDNA3.1-3x HA-FAAH 1-305 (residues 1-305) constructs were generated in the same vector background using Gibson assembly. The PCDNA3.1-3x Flag-NLRP3 expression clone was purchased from Sino Biological. NLRP3 expression constructs PCDNA3.1-3x Flag-NLRP3 1-90 (pyrin domain), PCDNA3.1-3x Flag-NLRP3 91-710 (NACHT domain), PCDNA3.1-3x Flag-NLRP3 711-1034 (LRR domain), PCDNA3.1-3x Flag-NACHT 293-710 (residues 293-710) and PCDNA3.1-3x Flag-NACHT 494-710 (residues 494-710) were generated in the same vector background using Gibson assembly. The PCDNA3.1-3x V5-NLRP3 expression clone, NLRP3 expression constructs PCDNA3.1-3x V5-NLRP3 1-90 (pyrin domain), PCDNA3.1-3x V5-NLRP3 91-710 (NACHT domain), PCDNA3.1-3x V5-NLRP3 711-1034 (LRR domain) was purchased from Tsingke. To interrogate domain specificity of FAAH and NLRP3, HEK293T cells were plated into 6-well tissue culture plates in 2 mL complete DMEM overnight, cells were transiently transfected with 1.25 μg of the full-length FAAH or NLRP3 construct in combination with 1.25 μg of one of the domain constructs of NLRP3 or FAAH using Lipofectamine-3000 (Invitrogen, L3000015) in Opti-MEM™ (Gibco, 31985088). Opti-MEM was replaced with DMEM with 10% FBS 8 h after transfection, and 24 h after transfection, cells were lysed with NP-40 lysis buffer with 1% protease inhibitor cocktail. Whole-cell lysates were centrifuged to separate the supernatant fraction, and the pellet fraction was further subjected to immunoprecipitation experiments. Antibodies for HA, Flag were used to detect FAAH and NLRP3 on immunoblots.

Point mutation studies

The PCDNA3.1-FAAH-3xHA expression clone was purchased from Sino Biological. The PCDNA3.1-FAAH-3xHA S241A were generated in the same vector background using Gibson assembly. The PCDNA3.1-3xFlag-NLRP3 expression clone was purchased from Sino Biological. PCDNA3.1-3xFlag-NLRP3 R258W, PCDNA3.1-3xFlag-NLRP3 T346M and PCDNA3.1-3xFlag-NLRP3 F521L were generated in the same vector background using Gibson assembly. To interrogate Amino acid specificity of FAAH and NLRP3, HEK293T cells were plated into 6-well plates in 2 mL complete DMEM overnight, cells were transiently transfected with 1.25 μg of the full-length FAAH or NLRP3 construct in combination with 1.25 μg of one of the Point mutation constructs of NLRP3 or FAAH using Lipofectamine-3000 (Invitrogen, L3000015) in Opti-MEM™ (Gibco, 31985088). Opti-MEM was replaced with DMEM with 10% FBS 8 h after transfection, and 24 h after transfection, cells were lysed with NP-40 lysis buffer with 1% protease inhibitor cocktail. Whole-cell lysates were centrifuged to separate the supernatant fraction, and the pellet fraction was further subjected to immunoprecipitation experiments.

Transcriptome sequencing

Transcriptome sequencing was performed according to manufacturer's instruction (Novogene https://www.novogene.com).

Reconstitution of FAAH, FAAH S241A, and FAAH 1–265 in FAAH−/− macrophages

The PCDNA3.1-FAAH-3xHA expression clone was purchased from Sino Biological. The PLVX-EF1a-mcherry Lentiviruses vector was purchased from YouBio, Lentiviral PLVX-EF1a-FAAH-3xHA, PLVX-EF1a-FAAH-S241A-3xHA and PLVX-EF1a-FAAH 1–265-3xHA constructs were generated in the same vector background using Gibson assembly. Bone marrow cells were collected from FAAH deficient mice and were transduced with lentivirus containing PLVX-EF1a-FAAH-3xHA, PLVX-EF1a-FAAH-S241A-3xHA or PLVX-EF1a-1–265-3xHA. Lentiviruses were packaged in HEK293T cells using packaging plasmids pMD2.G and psPAX2 in DMEM supplemented with 10% FBS. The supernatant of Lentiviruses was collected 48 and 72 h after transfection, concentrated by Lenti-X concentrator and stored at −80 °C. Expression of reconstituted proteins was determined by immunoblotting.

Separation of cytosol fractions and membrane fractions

BMDMs were washed with PBS and digested with Trypsin-EDTA (Gibco, 25200-072), then homogenized in isotonic buffer (0.25 M sucrose, 10 mM Tris-HCl (pH 7.5), 10 mM KCl, 1.5 mM $MgCl_2$ and protease inhibitor cocktail) and centrifuged at $1000 \times g$ for 5 min to remove nucleus pellet. The supernatant was further centrifuged at 100,000 g for 20 min to separate cytosol fraction and membrane fraction. Then collect the supernatant for cytosol fractions and the pellet for membrane fractions to Immunoblots.

Immunofluorescence staining and imaging

For immunostaining, the cells were fixed with 4% paraformaldehyde, then punched in PBS containing 0.5% TritonX-100, blocked with 0.5% BSA-PBS at room temperature for 1 h, and the primary antibody was added to incubate overnight at 4 °C. Incubated with AlexaFluor secondary antibody at room temperature for 1 h the next day, stained the cell nucleus with 0.5 μg/mL DAPI (Beyotime, C1006), dropped a fluorescence quencher, and observed the fluorescence under a confocal microscope Leica SP8 (Leica Microsystems).

Histopathologic section

The tissues of skin, axillary lymph node, liver and spleen were collected from sacrificed mice, soaked in 4% paraformaldehyde, made transparent with xylene, embedded in paraffin, sliced into thin sections, stained with hematoxylin & eosin (H&E), and finally sealed into slices for observation and analyzed with CaseViewer 2.0.

IHC

Axillary lymph node was harvested, paraffin embedded and processed by standard immunohistochemical protocol, then sectioned for F4/80 antibody staining.

Flow cytometry

Anti-CD45.2 and anti-GR-1 monoclonal antibodies were used for flow cytometry analyses. Data were acquired on a FACS Calibur flow cytometer (BD) and analyzed with FlowJo software (FlowJo and Illumina). For t-SNE analysis of multi-parameter flow cytometry data, liver CD45+ leukocytes were gated in FlowJo software (Version 10.6, Tree Star, Inc, Ashland, USA), and then the expression matrixes of CD45+ leukocytes from wildtype, *FAAH*$^{+/+}$ R258W, *FAAH*$^{+/-}$ R258W and *FAAH*$^{-/-}$ R258W mice were exported. Next, 3000 cells from four matrixes were randomly selected to merge into one single matrix which contained 12,000 cells and 16 channels in R language (version 3.5.3). Then, matrix was normalized by channel using a centered log ratio transformation (CLR) method embedded in NormalizeData function of Seurat package (Version 3.1.5). The t-SNE algorithm was run with the normalized expression matrix by RunTSNE function in Seurat package.

CAPS patients information

P1 was a 2 years old girl, and presented with recurrent fever and skin rash for over 1 year. She was diagnosed as FCAS. P2 was a 3 years old girl and developed recurrent skin rash after birth. At the age of 1 year old, she developed recurrent abdominal pain. Histology revealed intestinal inflammation. She was diagnosed as FCAS. P3 was a 7 months old boy, and presented recurrent fever and skin rash post birth. He developed aseptic meningitis at 4 months old, and arthritis at 6 months old, respectively. He was diagnosed as CINCA. All the patients had leukocytosis, increased erythrocyte sedimentation rate and C-reactive protein. Genetic study identified de novo heterozygous mutation of NLRP3 gene in the three patients (c.1060G>A, p.A354T in P1; c.1049C>T, p.T350M in P2; c.1223T>C, p.M408T in P3). Blood samples were collected with the informed consent from the three donors, and the experiment was ethically approved by the Department of Rheumatology and Immunology, Beijing Children's Hospital of Capital Medical University.

Isolation of murine Kupffer cells

The mice were sacrificed, the abdominal cavity was opened after skin disinfection, the portal vein was exposed, and liver perfusion was performed with 0.5 mM EGTA solution and added DMEM medium. Then the liver was shredded to form single-cell suspension. 0.075% collagenase Type IV (Gibco, 17104019) was added to the suspension, and the liver was digested on the shaking machine for 20 min at 80 rpm. The undigested tissue mass was removed through a 200-mesh screen, and centrifuged at $50 \times g$ for 5 min. The centrifugation was repeated twice. Centrifuged at $500 \times g$ for 10 min, and cell precipitation was collected. Cells were isolated with 25% and 50% Percoll™ (GE Healthcare,17-0891-09), 25% Percoll was slowly adhered to the wall and added over 50% Percoll, centrifuged at $800 \times g$ for 15 min (Set acceleration to 6 and Set deceleration to 2). The cells in the middle layer were collected and resuspended with DMEM medium and centrifuged at $500 \times g$ for 5 min and collected for cell counting. Then the cells were added to DMEM medium with 10% fetal bovine serum and 10% Penicillin–Streptomycin solution for culturing overnight.

Isolation and culture of PBMCs

Human peripheral blood mononuclear cells (PBMCs) were isolated by Ficoll-Paque™ PLUS (GE Healthcare, 17-1440-02) density gradient centrifugation. Buffy coat generated in the middle of the gradient was collected, mixed with PBS and spun at $100 \times g$ for 10 min. Cells were then washed twice with PBS and resuspended in RPMI 1640 supplemented with 10% FBS and incubated at 37 °C with 5% CO_2 overnight [45].

Statistics and reproducibility

GraphPad Prism 8.4.1 software was used for data analysis. Statistical significance was determined by unpaired two-tailed *t* test. Unless otherwise noted, the mean was used to represent central tendency, and error bars represent the standard error of the mean (s.e.m.). Unless otherwise noted, every experiment was done with at least three biologically independent replicates. $^{*}P < 0.05$; $^{**}P < 0.01$; $^{***}P < 0.001$. For ELISA data, values from multiple experiments were pooled together, which might have led to overlap of values between panels. Representative western blots and microscopy images are shown from at least three biologically independent replicates that showed similar results. No statistical methods were used to predetermine sample size and the experiments were not randomized. Western blotting was quantified using Image J.

DATA AVAILABILITY

All data are presented in the main text or Supplementary Materials. The expression plasmids reported in this paper are available upon request. The rest of the data supporting the present study are available from the corresponding author upon reasonable request.

REFERENCES

1. Evavold CL, Kagan JC. Inflammasomes: threat-assessment organelles of the innate immune system. Immunity 2019;51:609–24.
2. Broz P, Dixit VM. Inflammasomes: mechanism of assembly, regulation and signaling. Nat Rev Immunol. 2016;16:407–20.
3. Lamkanf M, Dixit VM. Mechanisms and functions of inflammasomes. Cell 2014;157:1013–22.
4. Mangan MSJ, Olhava EJ, Roush WR, Seidel HM, Glick GD, Latz E. Targeting the NLRP3 inflammasome in inflammatory diseases. Nat Rev Drug Discov. 2018;17:588–606.
5. Duewell P, Kono H, Rayner KJ, Sirois CM, Vladimer G, Bauernfeind FG, et al. NLRP3 inflammasomes are required for atherogenesis and activated by cholesterol crystals. Nature 2010;464:1357–61.
6. Martinon F, Petrilli V, Mayor A, Tardivel A, Tschopp J. Gout-associated uric acid crystals activate the NALP3 inflammasome. Nature 2006;440:237–41.
7. Swanson KV, Deng M, Ting JP. The NLRP3 inflammasome: molecular activation and regulation to therapeutics. Nat Rev Immunol. 2019;19:477–89.
8. Agostini L, Martinon F, Burns K, McDermott MF, Hawkins PN, Tschopp J. NALP3 forms an IL-1beta-processing inflammasome with increased activity in Muckle-Wells autoinflammatory disorder. Immunity 2004;20:319–25.
9. Man SM, Karki R, Kanneganti TD. Molecular mechanisms and functions of pyroptosis, inflammatory caspases and inflammasomes in infectious diseases. Immunol Rev. 2017;277:61–75.
10. Booshehri LM, Hoffman HM. CAPS and NLRP3. J Clin Immunol. 2019;39:277–86.
11. Aganna E, Martinon F, Hawkins PN, Ross JB, Swan DC, Booth DR, et al. Association of mutations in the NALP3/CIAS1/PYPAF1 gene with a broad phenotype including recurrent fever, cold sensitivity, sensorineural deafness, and AA amyloidosis. Arthritis Rheum. 2002;46:2445–52.
12. Aksentijevich I, Nowak M, Mallah M, Chae JJ, Watford WT, Hofmann SR, et al. De novo CIAS1 mutations, cytokine activation, and evidence for genetic heterogeneity in patients with neonatal-onset multisystem inflammatory disease (NOMID): a new member of the expanding family of pyrin-associated autoinflammatory diseases. Arthritis Rheum. 2002;46:3340–8.
13. Neven B, Callebaut I, Prieur AM, Feldmann J, Bodemer C, Lepore L, et al. Molecular basis of the spectral expression of CIAS1 mutations associated with phagocytic cell-mediated autoinflammatory disorders CINCA/NOMID, MWS, and FCU. Blood 2004;103:2809–15.
14. Meng G, Zhang F, Fuss I, Kitani A, Strober W. A mutation in the Nlrp3 gene causing inflammasome hyperactivation potentiates Th17 cell-dominant immune responses. Immunity 2009;30:860–74.
15. Gritsenko A, Green JP, Brough D, Lopez-Castejon G. Mechanisms of NLRP3 priming in inflammaging and age-related diseases. Cytokine Growth Factor Rev. 2020;55:15–25.
16. Song H, Liu B, Huai W, Yu Z, Wang W, Zhao J, et al. The E3 ubiquitin ligase TRIM31 attenuates NLRP3 inflammasome activation by promoting proteasomal degradation of NLRP3. Nat Commun. 2016;7:13727.
17. Shi CS, Shenderov K, Huang NN, Kabat J, Abu-Asab M, Fitzgerald KA, et al. Activation of autophagy by inflammatory signals limits IL-1beta production by targeting ubiquitinated inflammasomes for destruction. Nat Immunol. 2012;13:255–63.
18. Yan Y, Jiang W, Liu L, Wang X, Ding C, Tian Z, et al. Dopamine controls systemic inflammation through inhibition of NLRP3 inflammasome. Cell 2015;160:62–73.
19. Song H, Zhao C, Yu Z, Li Q, Yan R, Qin Y, et al. UAF1 deubiquitinase complexes facilitate NLRP3 inflammasome activation by promoting NLRP3 expression. Nat Commun. 2020;11:6042.
20. Liu T, Wang L, Liang P, Wang X, Liu Y, Cai J, et al. USP19 suppresses inflammation and promotes M2-like macrophage polarization by manipulating NLRP3 function via autophagy. Cell Mol Immunol. 2021;18:2431–42.
21. Zhou R, Yazdi AS, Menu P, Tschopp J. A role for mitochondria in NLRP3 inflammasome activation. Nature 2011;469:221–5.
22. Elliott EI, Miller AN, Banoth B, Iyer SS, Stotland A, Weiss JP, et al. Cutting edge: mitochondrial assembly of the NLRP3 inflammasome complex is initiated at priming. J Immunol. 2018;200:3047–52.
23. Hamilton C, Anand PK. Right place, right time: localization and assembly of the NLRP3 inflammasome. F1000Research. 2019; 8: F1000 Faculty Rev-676.
24. Subramanian N, Natarajan K, Clatworthy MR, Wang Z, Germain RN. The adaptor MAVS promotes NLRP3 mitochondrial localization and inflammasome activation. Cell 2013;153:348–61.

25. Iyer SS, He Q, Janczy JR, Elliott EI, Zhong Z, Olivier AK, et al. Mitochondrial cardiolipin is required for Nlrp3 inflammasome activation. Immunity 2013;39:311–23.
26. Ichinohe T, Yamazaki T, Koshiba T, Yanagi Y. Mitochondrial protein mitofusin 2 is required for NLRP3 inflammasome activation after RNA virus infection. Proc Natl Acad Sci USA. 2013;110:17963–8.
27. Wang W, Hu D, Wu C, Feng Y, Li A, Liu W, et al. STING promotes NLRP3 localization in ER and facilitates NLRP3 deubiquitination to activate the inflammasome upon HSV-1 infection. PLoS Pathog. 2020;16:e1008335.
28. McKinney MK, Cravatt BF. Structure and function of fatty acid amide hydrolase. Annu Rev Biochem. 2005;74:411–32.
29. Di Marzo V. New approaches and challenges to targeting the endocannabinoid system. Nat Rev Drug Disco. 2018;17:623–39.
30. Van Egmond N, Straub VM, van der Stelt M. Targeting endocannabinoid signaling: FAAH and MAG Lipase inhibitors. Annu Rev Pharm Toxicol. 2021;61:441–63.
31. Wang ZY, Wang PQ, Hillard CJ, Bjorling DE. Attenuation of cystitis and pain sensation in mice lacking fatty acid amide hydrolase. J Mol Neurosci. 2015;55:968–76.
32. Sałaga M, Mokrowiecka A, Zakrzewski PK, Cygankiewicz A, Leishman E, Sobczak M, et al. Experimental colitis in mice is attenuated by changes in the levels of endocannabinoid metabolites induced by selective inhibition of fatty acid amide hydrolase (FAAH). J Crohns Colitis. 2014;8:998–1009.
33. Eljaschewitsch E, Witting A, Mawrin C, Lee T, Schmidt PM, Wolf S, et al. The endocannabinoid anandamide protects neurons during CNS inflammation by induction of MKP-1 in microglial cells. Neuron 2006;49:67–79.
34. Su SH, Wu YF, Lin Q, Wang DP, Hai J. URB597 protects against NLRP3 inflammasome activation by inhibiting autophagy dysfunction in a rat model of chronic cerebral hypoperfusion. J Neuroinflammation. 2019;16:260.
35. Li G, Xia M, Abais JM, Boini K, Li PL, Ritter JK. Protective action of anandamide and its COX-2 metabolite against l-Homocysteine-induced NLRP3 inflammasome activation and injury in podocytes. J Pharm Exp Ther. 2016;358:61–70.
36. Cravatt BF, Demarest K, Patricelli MP, Bracey MH, Giang DK, Martin BR, et al. Supersensitivity to anandamide and enhanced endogenous cannabinoid signaling in mice lacking fatty acid amide hydrolase. Proc Natl Acad Sci USA. 2001;98:9371.
37. Wang H, Xie H, Guo Y, Zhang H, Takahashi T, Kingsley PJ, et al. Fatty acid amide hydrolase deficiency limits early pregnancy events. J Clin Investig. 2006;116:2122–31.
38. Gatica D, Lahiri V, Klionsky DJ. Cargo recognition and degradation by selective autophagy. Nat Cell Biol. 2018;20:233–42.
39. Patricelli MP, Cravatt BF. Clarifying the catalytic roles of conserved residues in the amidase signature family. J Biol Chem. 2000;275:19177–84.
40. Tripathi RKP. A perspective review on fatty acid amide hydrolase (FAAH) inhibitors as potential therapeutic agents. Eur J Med Chem. 2020;188:111953.
41. Fazio D, Criscuolo E, Piccoli A, Barboni B, Fezza F, Maccarrone M, et al. Advances in the discovery of fatty acid amide hydrolase inhibitors: what does the future hold. Expert Opin Drug Discov. 2020;15:765–78.
42. Vande Walle L, Stowe IB, Šácha P, Lee BL, Demon D, Fossoul A, et al. MCC950/CRID3 potently targets the NACHT domain of wild-type NLRP3 but not disease-associated mutants for inflammasome inhibition. PLoS Biol. 2019;17:e3000354.
43. Cravatt BF, Saghatelian A, Hawkins EG, Clement AB, Bracey MH, Lichtman AH. Functional disassociation of the central and peripheral fatty acid amide signaling systems. Proc Natl Acad Sci USA. 2004;101:10821–6.
44. Dainese E, Oddi S, Simonetti M, Sabatucci A, Angelucci CB, Ballone A, et al. The endocannabinoid hydrolase FAAH is an allosteric enzyme. Sci Rep. 2020;10:2292.
45. Mehto S, Jena KK, Nath P, Chauhan S, Kolapalli SP, Das SK, et al. The Crohn's disease risk factor IRGM limits NLRP3 inflammasome activation by impeding its assembly and by mediating its selective autophagy. Mol Cell. 2019;73:429–45.e7.

ACKNOWLEDGEMENTS

We thank Dr. Warren Strober for sharing the *Nlrp3*^{R258W} mouse line and Prof. Zhexiong Lian for assistance on mice studies.

AUTHOR CONTRIBUTIONS

YYZ, ZH, HWM, SQZ, YBH, SRC, YK, ZBZ, XHH, ZY, YH, XWH, MMW, and WBZ performed the experiments; LJ, and GXM designed the research; XHQ, ZMY, JNS, SY, and YCX wrote the paper; LSW, YJZ, and LPW supervised the project.

FUNDING

This work was supported by National Natural Science Foundation of China (82150118, 32171375, 32071398, T2222014), Key-Area Research and Development Program of Guangdong Province (2020B0101030006, 2020B1515120096, 2022B0202010002), the Program for Guangdong Introducing Innovative and Entrepreneurial Teams (2017ZT07S054), and the Natural Science Foundation for Distinguished Young Scholars of Guangdong Province (2018B030306035).

COMPETING INTERESTS

The authors declare no competing interests.

ETHICS APPROVAL

All mice were housed in a specific pathogen-free facility in the Laboratory Animal Center of South China University of Technology. The experiments using patient-derived PBMCs have complied with all relevant ethical regulations with the informed consent from the patients. The experiment was ethically approved by the Department of Rheumatology and Immunology, Beijing Children's Hospital of Capital Medical University.

ADDITIONAL INFORMATION

Supplementary information The online version contains supplementary material available at https://doi.org/10.1038/s41418-022-01054-4.

Correspondence and requests for materials should be addressed to Liansheng Wang, Yunjiao Zhang or Longping Wen.